AIAA JOURNAL
Vol. 47, No. 12, December 2009

Interaction of Microwave-Generated Plasma with a Hemisphere Cylinder at Mach 2.1

Doyle Knight*
Rutgers, The State University of New Jersey, New Brunswick, New Jersey 08903
Yuri F. Kolesnichenko,† Vadim Brovkin,‡ and Dmitri Khmara§
Russian Academy of Sciences, 127412, Moscow, Russia
and
Valery Lashkov¶ and Igor Mashek**
St. Petersburg State University, 198504, St. Petersburg, Russia

DOI: 10.2514/1.43657

Microwave energy deposition is a novel method for flow control in high-speed flows. Experiments have demonstrated its capability for beneficial flowfield modification in supersonic flow including, for example, drag reduction for blunt bodies. A fully three-dimensional, time-accurate gas dynamic code has been developed for simulating microwave energy deposition in air and the interaction of the microwave-generated plasma with the supersonic flow past a blunt body. The thermochemistry model includes 23 species and 238 reactions. The code is applied to the simulation of microwave energy deposition in supersonic flow past a hemisphere cylinder. The computed centerline surface pressure is compared with the experiment. The interaction of the microwave-generated plasma with the flowfield structure is examined.

Nomenclature

c_{p_i}	=	specific heat at constant pressure for species i
D	=	diameter of cylinder
E, E_o	=	electric field, maximum electric field
H	=	total enthalpy per unit mass of mixture
$h^o_{f_i}$	=	heat of formation of species i at temperature T_{ref}
h_i	=	static enthalpy of species i per unit mass of species i
h	=	static enthalpy per unit mass of mixture
K_k	=	reaction coefficient for reaction k
k	=	Boltzmann constant, 1.38×10^{-23} J/K
k_E	=	microwave wave number, $=2\pi/\lambda$
M	=	representative mass for ions and neutrals
M_i	=	molecular weight of species i, kg/kg · mol
$\mathcal{M}_i$	=	species i (e.g., $\mathcal{M}_1 = e$)
M_∞	=	Mach number
m	=	number of reactions
m_e	=	mass of electron
$\mathcal{N}$	=	total concentration of species excluding electrons, cm^{-3}
N_e, N_e^{crit}	=	electron concentration, critical electron concentration, cm^{-3}
N_i	=	concentration of species i, cm^{-3}
n	=	number of species including electrons
p	=	static pressure
$\dot{p}_{i_k}$	=	rate of production of species i from reaction k

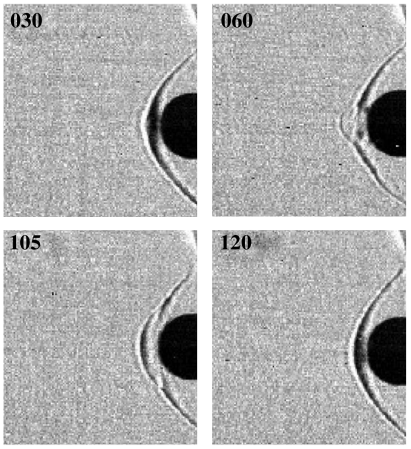

Fig. 1 Interaction of microwave-generated plasma with cylinder.

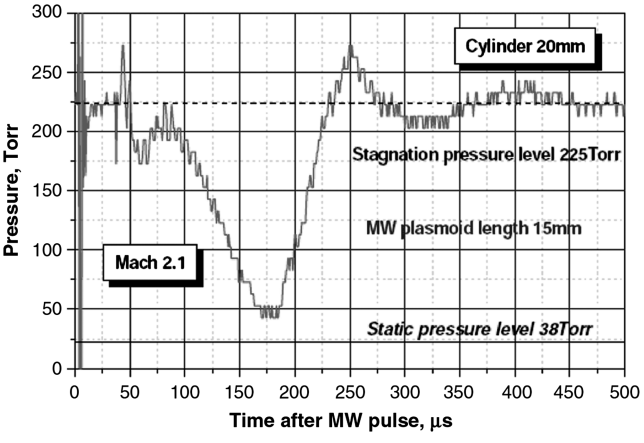

Fig. 2 Centerline pressure vs time.

Presented as Paper 0846 at the AIAA 47th Aerospace Sciences Meeting, Orlando, FL, 5–9 January 2009; received 5 February 2009; revision received 4 August 2009; accepted for publication 4 August 2009.

*Professor, Department of Mechanical and Aerospace Engineering. Associate Fellow AIAA.
†Chief of Laboratory, Department of Magnetohydrodynamics and Low Temperature Plasma, Joint Institute of High Temperatures. Member AIAA.
‡Chief Scientist, Microwave Discharge and Diagnostics, Joint Institute of High Temperatures.
§Deceased.
¶Head of Stationary Gas Dynamics Research Group, Research Institute of Mathematics and Mechanics.
**Professor of General Physics, Physical Department.

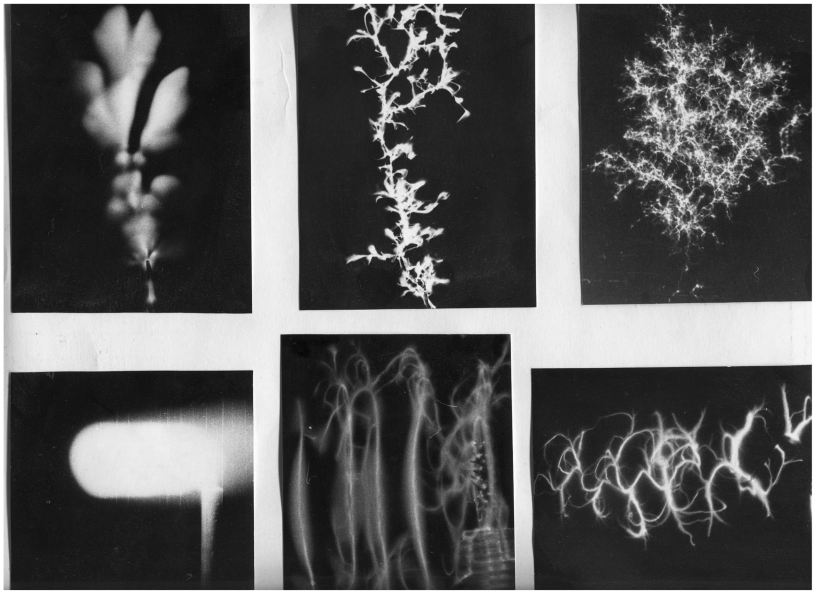

Fig. 3 Examples of microwave discharge.

$\dot{q}$ = rate of heating of gas per unit volume
$\mathcal{R}$ = universal gas constant, 8314 J/kg · mol K
T = static (translational) temperature of mixture
T_e = electron temperature
u_i = mass-averaged velocity component in i direction
V_{dr} = drift velocity
x_i = Cartesian coordinate
Y_i = mass fraction of species i, $Y_i = \rho_i/\rho$
α_i = fraction of Δh_i converted into heating of gas
Δh_i = rate of change in enthalpy due to reaction i
δ = $2m_e/M$
ε = total energy per unit mass of mixture
λ = wavelength of microwave
ν = rotational relaxation factor, dimensionless
ν_e = effective frequency of electron collisions
ν'_{ik}, ν''_{ik} = reaction coefficients
ρ_i, ρ = density of species i, density of mixture

Table 1 Reactions depending on T, part 1

Reactions	A	n	B
Excited states chemistry			
$N_2(a'^1\Sigma_u^-) + N_2(a'^1\Sigma_u^-) \rightarrow N_4^+ + e$	5.00E − 12	0.00	0.0
$N_2(a'^1\Sigma_u^-) + N_2(a'^1\Sigma_u^-) \rightarrow N_2 + N_2^+ + e$	2.00E − 10	0.00	0.0
$N_2(A^3\Sigma_u^+) + N_2(a'^1\Sigma_u^-) \rightarrow N_4^+ + e$	6.00E − 12	0.00	0.0
$N(^2P) + N(^2D) \rightarrow N_2^+ + e$	1.00E − 12	0.00	0.0
$N(^2P) + N(^2P) \rightarrow N_2^+ + e$	5.00E − 12	0.00	0.0
$N_2(a'^1\Sigma_u^-) + N_2 \rightarrow N_2 + N_2$	2.15E − 13	0.00	0.0
$N_2(a'^1\Sigma_u^-) + N_2 \rightarrow N_2(B^3\Pi_g) + N_2$	2.00E − 13	0.00	0.0
$N_2(a'^1\Sigma_u^-) + N_2 \rightarrow N_2(A^3\Sigma_u^+) + N_2$	2.00E − 13	0.00	0.0
$N_2(a'^1\Sigma_u^-) + N \rightarrow N_2 + N(^2P)$	1.00E − 10	0.00	0.0
$N_2(a'^1\Sigma_u^-) + O_2 \rightarrow N_2 + O + O$	2.80E − 11	0.00	0.0
$N_2(a'^1\Sigma_u^-) + NO \rightarrow N_2 + N + O$	3.60E − 10	0.00	0.0
$N_2(a'^1\Sigma_u^-) + O_2^- \rightarrow O_2 + N_2 + e$	5.00E − 09	0.00	0.0
$N_2(A^3\Sigma_u^+) + N \rightarrow N_2 + N(^2P)$	7.20E − 06	−2.10	0.0
$N_2(A^3\Sigma_u^+) + N_2 \rightarrow N_2(B^3\Pi_g) + N_2$	1.00E − 11	0.00	0.0
$N_2(A^3\Sigma_u^+) + N_2(A^3\Sigma_u^+) \rightarrow N_2(B^3\Pi_g) + N_2$	1.11E − 03	−2.64	0.0
$N_2(A^3\Sigma_u^+) + N_2(A^3\Sigma_u^+) \rightarrow N_2(C^3\Pi_u) + N_2$	2.77E − 04	−2.64	0.0
$N_2(A^3\Sigma_u^+) + N_2(B^3\Pi_g) \rightarrow N_2(C^3\Pi_u) + N_2$	4.60E − 10	0.00	0.0
$N_2(A^3\Sigma_u^+) + O_2 \rightarrow N_2 + O + O$	1.04E − 13	0.55	0.0
$N_2(A^3\Sigma_u^+) + O \rightarrow N_2 + O$	5.80E − 12	0.00	0.0
$N_2(A^3\Sigma_u^+) + O \rightarrow N_2 + O(^1S)$	1.73E − 11	0.00	0.0
$N_2(A^3\Sigma_u^+) + NO \rightarrow N_2 + NO$	3.10E − 11	0.00	0.0
$N_2(A^3\Sigma_u^+) + NO \rightarrow N_2 + N + O$	8.80E − 12	0.00	0.0
$N_2(A^3\Sigma_u^+) + O^- \rightarrow O + N_2 + e$	2.10E − 09	0.00	0.0
$N_2(A^3\Sigma_u^+) + O^- \rightarrow NO + N + e$	1.00E − 10	0.00	0.0
$N_3(A^3\Sigma_u^+) + O_2^- \rightarrow e + N_2 + O_2$	2.10E − 09	0.00	0.0
$N_2(B^3\Pi_g) + N_2 \rightarrow N_2(A^3\Sigma_u^+) + N_2$	2.20E − 11	0.00	0.0
$N_2(B^3\Pi_g) + N \rightarrow N_2 + N(^2P)$	1.00E − 10	0.00	0.0
$N_2(B^3\Pi_g) + N_2 \rightarrow N_2 + N_2$	4.60E − 12	0.00	0.0
$N_2(B^3\Pi_g) + O_2 \rightarrow N_2 + O + O$	3.00E − 10	0.00	0.0
$N_2(B^3\Pi_g) + O_2 \rightarrow N_2(A^3\Sigma_u^+) + O_2$	2.70E − 11	0.00	0.0
$N_2(B^3\Pi_g) + O_2^- \rightarrow e + N_2 + O_2$	2.50E − 09	0.00	0.0
$N_2(B^3\Pi_g) + O^- \rightarrow e + N_2 + O$	1.90E − 09	0.00	0.0

Table 2 Reactions depending on T, part 2

Reactions	A	n	B
Excited states chemistry			
$N_2(C^3\Pi_u) + N \rightarrow N_2(B^3\Pi_g) + N$	2.30E − 11	0.00	0.0
$N_2(C^3\Pi_u) + N \rightarrow N_2 + N(^2P)$	1.00E − 10	0.00	0.0
$N_2(C^3\Pi_u) + N_2 \rightarrow N_2 + N_2$	2.30E − 11	0.00	0.0
$N_2(C^3\Pi_u) + N_2 \rightarrow N_2(A^3\Sigma_u^+) + N_2$	3.00E − 10	0.00	0.0
$N_2(C^3\Pi_u) + N_2 \rightarrow N_2(a'^1\Sigma_u^-) + N_2$	1.50E − 12	0.00	0.0
$N_2(C^3\Pi_u) + N_2 \rightarrow N_2(B^3\Pi_g) + N_2$	1.00E − 11	0.00	0.0
$N_2(C^3\Pi_u) \rightarrow N_2(B^3\Pi_g)$	2.73E + 07	0.00	0.0
$N_2(C^3\Pi_u) + O_2 \rightarrow N_2 + O(^1D) + O(^1D)$	2.03E − 10	0.00	0.0
$N_2(C^3\Pi_u) + O_2 \rightarrow N_2 + O + O(^1D)$	1.26E − 11	0.00	0.0
$N_2(C^3\Pi_u) + O \rightarrow NO + N$	7.00E − 12	0.00	0.0
$N_2(C^3\Pi_u) + NO \rightarrow N_2 + N + O$	2.00E − 11	0.00	0.0
$N(^2P) + N \rightarrow N(^2D) + N$	6.00E − 13	0.00	0.0
$N(^2P) + O \rightarrow N(^2D) + O$	2.70E − 11	0.00	0.0
$N(^2P) + O_2 \rightarrow N + O_2$	6.00E − 14	0.00	0.0
$N(^2P) + O_2 \rightarrow NO + O$	1.00E − 12	0.00	60.0
$N(^2P) + O_2 \rightarrow NO + O(^1D)$	1.00E − 12	0.00	60.0
$N(^2P) + O_2 \rightarrow NO + O(^1S)$	1.00E − 12	0.00	60.0
$N(^2P) + NO \rightarrow N + NO$	2.90E − 11	0.00	0.0
$N(^2D) + O_2 \rightarrow NO + O$	2.33E − 12	0.00	185.0
$N(^2D) + O_2 \rightarrow NO + O(^1D)$	7.37E − 12	0.00	185.0
$N(^2D) + O \rightarrow N + O(^1D)$	3.33E − 12	0.00	259.0
$N(^2D) + NO \rightarrow N_2 + O$	6.00E − 11	0.00	0.0
$N(^2D) + O^+ \rightarrow N^+ + O$	1.30E − 10	0.00	0.0
$N(^2D) + N_2 \rightarrow N_2 + N$	7.30E − 13	0.00	1065.0
$N(^2D) + N + N_2 \rightarrow N_2 + N_2(B^3\Pi_g)$	4.53E − 34	0.00	−500.0
$N(^2D) + N + N_2 \rightarrow N_2 + N_2(a'^1\Sigma_u^-)$	3.21E − 34	0.00	−500.0
$O(^1D) + O \rightarrow O + O$	1.20E − 11	0.00	0.0
$O(^1D) + O_2 \rightarrow O + O_2$	3.20E − 11	0.00	−67.0
$O(^1D) + N_2 \rightarrow O + N_2$	1.80E − 11	0.00	−107.0
$O(^1D) + NO \rightarrow O_2 + N$	4.50E − 11	0.00	0.0
$O(^1D) + NO \rightarrow NO + O$	4.00E − 11	0.00	0.0
$O(^1D) + N_2 + O \rightarrow N_2 + O_2$	9.94E − 33	0.00	0.0
$O(^1S) + O \rightarrow O + O(^1D)$	5.00E − 11	0.00	300.0
$O(^1S) + O_2 \rightarrow O_2 + O$	4.30E − 12	0.00	850.0

Table 3 Reactions depending on T, part 3

Reactions	A	n	B
High temperature dissociation			
$O_2 + N_2 \rightarrow O + O + N_2$	9.20E − 09	0.00	59380.0
$O_2 + N \rightarrow O + O + N$	9.20E − 09	0.00	59380.0
$O_2 + O_2 \rightarrow O + O + O_2$	3.70E − 08	0.00	59380.0
$O_2 + O \rightarrow O + O + O$	1.30E − 07	0.00	59380.0
O + O recombination			
$O + O + N \rightarrow O_2 + N$	6.50E − 35	0.00	−1040.0
$O + O + N \rightarrow NO + O$	5.51E − 27	−1.50	0.0
$O + O + O \rightarrow O_2 + O$	8.60E − 31	−0.63	0.0
$O + O + O_2 \rightarrow O_2 + O_2$	2.40E − 31	−0.63	0.0
N + N recombination			
$N + N + O \rightarrow N_2 + O$	3.03E − 32	−0.50	0.0
$N + N + O \rightarrow N + NO$	5.51E − 27	−1.50	0.0
$N + N + O_2 \rightarrow N_2(A^3\Sigma_u^+) + O_2$	8.27E − 34	0.00	−500.0
$N + N + N_2 \rightarrow N_2 + N_2$	5.60E − 35	0.00	−500.0
$N + N + N_2 \rightarrow N_2 + N_2(A^3\Sigma_u^+)$	3.21E − 34	0.00	−500.0
N + O recombination			
$N + O + N_2 \rightarrow N_2 + NO$	1.80E − 31	−0.50	0.0
$N + O + O_2 \rightarrow NO + O_2$	1.80E − 31	−0.50	0.0
N and NO reactions			
$N + O_2 \rightarrow NO + O$	1.50E − 14	1.00	3263.0
$NO + N \rightarrow N_2 + O$	3.51E − 11	0.00	50.0
Associative ionization			
$N + O \rightarrow NO^+ + e$	9.10E − 12	0.50	32000.0
$N + O(^1D) \rightarrow NO^+ + e$	9.10E − 12	0.50	9150.0
$N + O(^1S) \rightarrow NO^+ + e$	1.22E − 10	0.17	0.0
$N(^2D) + O \rightarrow NO^+ + e$	9.10E − 12	0.50	4860.0
$N(^2P) + O \rightarrow NO^+ + e$	2.70E − 11	0.00	0.0
Electron detachment			
$O^- + N_2 \rightarrow N_2 + O + e$	4.00E − 13	1.00	16900.0
$O^- + N \rightarrow NO + e$	2.40E − 10	0.00	0.0
$O_2^- + N \rightarrow NO + O + e$	4.00E − 10	0.00	0.0
$O_2^- + N_2 \rightarrow N_2 + O_2 + e$	5.10E − 17	1.50	5000.0
$O^- + O \rightarrow O_2 + e$	2.40E − 10	0.00	0.0
$O_2^- + O_2 \rightarrow O_2 + O_2 + e$	2.00E − 15	1.73	5000.0
$O_3^- + O \rightarrow O_2 + O_2 + e$	1.00E − 13	0.00	0.0
$O_3^- + O(^1D) \rightarrow O_2 + O_2 + e$	1.00E − 11	0.00	0.0
$O_3^- + O(^1S) \rightarrow O_2 + O_2 + e$	1.00E − 11	0.00	0.0

Table 4 Reactions depending on T, part 4

Reactions	A	n	B
Ion–ion recombination			
$O^+ + O^- + N_2 \rightarrow N_2 + O_2$	3.10E − 19	−2.50	0.0
$N^+ + O^- \rightarrow N + O$	4.50E − 06	−0.50	0.0
$N^+ + O^- + N_2 \rightarrow N_2 + NO$	3.10E − 19	−2.5	0.0
$N^+ + O^- + O_2 \rightarrow NO + O_2$	3.10E − 19	−2.50	0.0
$N^+ + O_2^- \rightarrow N + O_2$	3.46E − 06	−0.50	0.0
$N^+ + O_3^- \rightarrow NO + O_2$	7.00E − 07	−0.50	0.0
$N_2^+ + O^- \rightarrow NO + N$	2.60E − 06	−0.50	0.0
$N_2^+ + O^- \rightarrow N_2 + O$	1.75E − 06	−0.50	0.0
$N_2^+ + O_2^- \rightarrow N_2 + O_2$	2.60E − 06	−0.50	0.0
$N_4^+ + O^- \rightarrow N_2 + N_2 + O$	1.60E − 06	−0.50	0.0
$N_4^+ + O_2^- \rightarrow N_2 + N_2 + O_2$	2.20E − 06	−0.50	0.0
$NO^+ + O^- \rightarrow NO + O$	1.70E − 06	−0.50	0.0
$NO^+ + O_2^- \rightarrow NO + O_2$	2.60E − 06	−0.50	0.0
$O^+ + O_2^- \rightarrow O + O_2$	3.10E − 06	−0.50	0.0
$O^+ + O_3^- \rightarrow O_2 + O_2$	1.60E − 06	−0.50	0.0
$O_2^+ + O^- \rightarrow O_2 + O$	1.70E − 06	−0.50	0.0
$O_2^+ + O_2^- \rightarrow O_2 + O_2$	2.50E − 06	−0.50	0.0
Complex positive ions formation			
$N_2^+ + N_2 + N_2 \rightarrow N_4^+ + N_2$	6.10E − 27	−0.75	0.0
$N_2^+ + N_2 + N \rightarrow N_4^+ + N$	1.50E − 26	−1.00	0.0
$N_2^+ + N_2 + O_2 \rightarrow N_4^+ + O_2$	5.60E − 27	−0.75	0.0
$N_2^+ + N_2 + O \rightarrow N_4^+ + O$	4.40E − 27	−0.75	0.0
Complex positive ions decomposition			
$N_4^+ + N(^2P) \rightarrow N_2^+ + N_2 + N$	1.00E − 10	0.00	0.0
Complex negative ions formation			
$O^- + O_2 + N_2 \rightarrow O_3^- + N_2$	6.80E − 29	−0.75	0.0
$O^- + O_2 + O_2 \rightarrow O_3^- + O_2$	6.30E − 29	−0.75	0.0
$O^- + O_2 + O \rightarrow O_3^- + O$	5.60E − 29	−0.75	0.0
Complex negative ions decomposition			
$O_3^- + N(^2D) \rightarrow O^- + O_2 + N$	1.00E − 10	0.00	0.0
$O_3^- + N(^2P) \rightarrow O^- + O_2 + N$	1.00E − 10	0.00	0.0
$O_3^- + O(^1D) \rightarrow O^- + O_2 + O$	1.00E − 10	0.00	0.0
$O_3^- + O(^1S) \rightarrow O^- + O_2 + O$	1.00E − 10	0.00	0.0
Negative ions charge transfer			
$O + O + N_2 \rightarrow O_2 + N_2$	6.50E − 35	0.00	−1040.0
$O_2^- + O \rightarrow O^- + O_2$	3.30E − 10	0.00	0.0
$O_3^- + O \rightarrow O_2^- + O_2$	1.00E − 11	0.00	0.0

τ_o, τ_1 = time scales in microwave discharge
ω = microwave angular frequency
$\dot{\omega}_i$ = net rate of production of species i

I. Introduction

ELECTROMAGNETIC local flow control (ELFC) is a rapidly developing field of high-speed flow control in aerodynamics. In contrast to conventional mechanical or passive flow control techniques (see, for example, Cattafesta et al. [1] for examples of conventional flow control applied to flow-induced cavity oscillations), ELFC uses electromagnetic energy deposition (e.g., electron beam, laser, microwave, dc discharge, and dielectric barrier discharge) to achieve beneficial modification of the flowfield. ELFC has distinct advantages compared to conventional mechanical or electromechanical flow control systems. ELFC has a virtually instantaneous activation (on the order of nanoseconds compared to hundreds of milliseconds for mechanical or electromechanical devices). This is particularly important in hypersonic aerodynamics. ELFC also has the capability for action at a distance through beamed energy deposition (e.g., electron beam, laser, microwave). Annual conferences and workshops on ELFC have been organized in the United States and Russia since 1997 by the AIAA, the Joint Institute of High Temperatures in Moscow, and the Leninetz Holding Company in St. Petersburg, Russia. The proceedings of the aforementioned conferences, together with recent reviews [2–5], have illustrated the wide advantages of ELFC for aerodynamic drag reduction.

An example of the interaction of a microwave-generated plasma [6] with the flowfield of a blunt body is shown in the Schlieren images in Fig. 1. A hemisphere cylinder is aligned with the oncoming flow at Mach 2.1. A microwave pulse is focused upstream of the blunt body shock to create a plasma. The typical pulse duration is 1 or 2 ms. The sequence of images in Fig. 1 (where the time since the microwave pulse is indicated in microseconds in the number at the upper left of each image) displays the initial interaction at $t = 30$ μs when the plasma begins to interact with the blunt body shock. This interaction causes a lensing forward (i.e., upstream) of the blunt body shock, and the formation of a toroidal vortex between the shock and the blunt body. This toroidal vortex acts as an effective streamlining of the flow and momentarily reduces the surface pressure. The flowfield relaxes to its initial undisturbed state after approximately 100 μs.

An example of direct experimental evidence for (frontal) drag reduction of blunt bodies by interaction of a microwave-generated plasma is shown in Fig. 2 from Kolesnichenko et al. [7]. The centerline pressure on a blunt cylinder at Mach 2.1 is shown as a function of time during the interaction of the microwave-generated plasma with the blunt body shock associated with the cylinder. The surface centerline pressure is reduced to nearly the freestream static pressure resulting in a net momentary decrease in (frontal) drag. Additional experiments have been performed for different geometries and confirmed the capability for drag reduction.

The modeling of a microwave-generated plasma and its interaction with an aerodynamic body is a complex task. Figure 3 displays the instantaneous images of different microwave discharges in air and illustrates the complex structures formed [8]. In particular, the thin "streamers" constitute an important aspect of the discharge because their temperature is substantially greater than the surrounding cooler plasma and consequently have greater influence when the plasma interacts with a blunt body shock wave, for example. Streamers aligned with the flow and centerline of a blunt cylinder have been observed experimentally to cause a significant momentary drag reduction (Fig. 2); however, streamers whose axis is significantly

Table 5 Reactions depending on T, part 5

Reactions	A	n	B
Positive ions charge transfer			
$O^+ + N \rightarrow N^+ + O$	2.20E − 09	0.00	10900.0
$O^+ + N_2 \rightarrow NO^+ + N$	1.20E − 12	0.00	0.0
$O^+ + NO \rightarrow NO^+ + O$	1.00E − 09	0.00	0.0
$O^+ + NO \rightarrow N + O_2^+$	3.00E − 12	0.00	0.0
$O^+ + O + N_2 \rightarrow N_2 + O_2^+$	1.70E − 27	−2.50	0.0
$O^+ + N + O \rightarrow NO^+ + O$	4.53E − 29	−0.75	0.0
$O^+ + N + N \rightarrow NO^+ + N$	5.58E − 29	−0.75	0.0
$O^+ + N + N_2 \rightarrow NO^+ + N_2$	5.80E − 29	−0.75	0.0
$O^+ + N + O_2 \rightarrow NO^+ + O_2$	5.30E − 29	−0.75	0.0
$O_2^+ + N \rightarrow NO^+ + O$	1.20E − 10	0.00	0.0
$O_2^+ + N_2 \rightarrow NO^+ + NO$	1.00E − 17	0.00	0.0
$O_2^+ + NO \rightarrow O_2 + NO^+$	4.30E − 10	0.00	0.0
$N^+ + O \rightarrow N + O^+$	5.00E − 10	0.00	0.0
$N^+ + O_2 \rightarrow N + O_2^+$	3.11E − 10	0.00	0.0
$N^+ + O_2 \rightarrow NO^+ + O$	2.63E − 10	0.00	0.0
$N^+ + O_2 \rightarrow NO + O^+$	3.66E − 11	0.00	0.0
$N^+ + NO \rightarrow N + NO^+$	4.51E − 10	0.00	0.0
$N^+ + NO \rightarrow N_2^+ + O$	7.90E − 11	0.00	0.0
$N^+ + NO \rightarrow N_2 + O^+$	1.00E − 12	0.00	0.0
$N^+ + O + N \rightarrow NO^+ + N$	4.37E − 29	−0.75	0.0
$N^+ + O + O \rightarrow NO^+ + O$	3.55E − 29	−0.75	0.0
$N^+ + O + N_2 \rightarrow N_2 + NO^+$	7.20E − 28	−0.75	0.0
$N^+ + O + O_2 \rightarrow NO^+ + O_2$	7.20E − 28	−0.75	0.0
$N^+ + N + O_2 \rightarrow N_2^+ + O_2$	7.20E − 28	−0.75	0.0
$N_2^+ + O \rightarrow N_2 + O^+$	3.13E − 11	−0.20	0.0
$N_2^+ + O \rightarrow NO^+ + N$	2.25E − 09	−0.50	0.0
$N_2^+ + O \rightarrow NO + N^+$	3.00E − 10	0.00	25800.0
$N_2^+ + O_2 \rightarrow N_2 + O_2^+$	1.04E − 09	−0.50	0.0
$N_2^+ + O_2 \rightarrow NO + NO^+$	3.00E − 14	0.00	0.0
$N_2^+ + N \rightarrow N^+ + N_2$	4.00E − 10	0.00	0.0
$N_2^+ + NO \rightarrow N_2 + NO^+$	3.30E − 10	0.00	0.0
$N_4^+ + O_2 \rightarrow O_2^+ + N_2 + N_2$	3.35E − 10	0.00	0.0
$N_4^+ + O \rightarrow O^+ + N_2 + N_2$	2.50E − 10	0.00	0.0
$N_4^+ + NO \rightarrow N_2 + N_2 + NO^+$	4.00E − 10	0.00	0.0
$N_4^+ + N_2 \rightarrow N_2^+ + N_2 + N_2$	7.10E − 24	3.80	1084.0
$NO^+ + O_2 \rightarrow NO + O_2^+$	1.09E − 09	−0.04	35560.0
$NO^+ + NO \rightarrow N_2 + O_2^+$	5.31E − 16	0.00	11900.0
$O^+ + O_2 \rightarrow O_2^+ + O$	1.90E − 11	0.00	0.0
$O^+ + O + O_2 \rightarrow O_2^+ + O_2$	1.70E − 27	−2.50	0.0

Table 6 Reactions depending on T_e

Reaction	A	n	B
Electron–ion recombination			
$e + N_2^+ \rightarrow N + N(^2D)$	4.07E − 07	−0.30	0.0
$e + N_2^+ \rightarrow N(^2D) + N(^2D)$	4.75E − 07	−0.30	0.0
$e + N_2^+ \rightarrow N + N(^2P)$	8.73E − 08	−0.30	0.0
$e + N_4^+ \rightarrow N_2 + N_2(A^3\Sigma_u^+)$	4.50E − 06	−0.50	0.0
$e + N_4^+ \rightarrow N_2 + N_2(B^3\Pi_g)$	4.50E − 06	−0.50	0.0
$e + N_4^+ \rightarrow N_2 + N_2(C^3\Pi_u)$	4.50E − 05	−0.50	0.0
$e + N^+ + O_2 \rightarrow N + O_2$	9.35E − 21	−2.50	0.0
$e + N_2^+ + O_2 \rightarrow N_2 + O_2$	9.35E − 21	−2.50	0.0
$e + O_2^+ + N_2 \rightarrow O_2 + N_2$	1.56E − 20	−2.50	0.0
$e + NO^+ \rightarrow N + O$	1.50E − 06	−0.50	0.0
$e + NO^+ \rightarrow N(^2D) + O$	1.50E − 06	−0.50	0.0
$e + NO^+ + N_2 \rightarrow NO + N_2$	9.35E − 21	−2.50	0.0
$e + NO^+ + O_2 \rightarrow NO + O_2$	9.35E − 21	−2.50	0.0
$e + e + NO^+ \rightarrow NO + e$	1.40E − 08	−4.50	0.0
$e + O^+ + N_2 \rightarrow O + N_2$	7.86E − 16	−4.50	0.0
$e + O^+ + O_2 \rightarrow O + O_2$	9.35E − 21	−2.50	0.0
$e + e + O^+ \rightarrow e + O$	1.40E − 08	−4.50	0.0
$e + O_2^+ \rightarrow O(^1D) + O$	6.24E − 06	−0.70	0.0
$e + O_2^+ \rightarrow O(^1D) + O(^1D)$	3.90E − 06	−0.70	0.0
$e + O_2^+ \rightarrow O + O$	2.86E − 06	−0.70	0.0
$e + O_2^+ + O_2 \rightarrow O_2 + O_2$	1.25E − 22	−2.50	0.0
Electron attachment			
$e + O + N \rightarrow N + O^-$	5.51E − 30	−0.50	0.0
$e + O + N_2 \rightarrow N_2 + O^-$	5.51E − 30	−0.50	0.0
$e + O_2 + N_2 \rightarrow O_2^- + N_2$	1.13E − 28	−0.90	1000.0
$e + O_2 + O_2 \rightarrow O_2^- + O_2$	6.00E − 27	−0.90	1000.0
$e + O_2 + O \rightarrow O_2^- + O$	2.76E − 32	0.00	0.0
$e + O + O_2 \rightarrow O^- + O_2$	5.51E − 30	−0.50	0.0
$e + O + O \rightarrow O^- + O$	1.43E − 29	−0.50	0.0

displaced compared to the centerline of the cylinder have been observed experimentally to result in a momentary drag increase [6].

The principal effect of the interaction of a microwave-generated plasma with the flowfield surrounding a blunt body is thermal, that is, the effect of the interaction of a finite heated region with the flowfield structure (e.g., shock waves, expansions) generated by the aerodynamic body. Validation of this statement is provided by numerous ideal gas simulations (e.g., Georgievsky and Levin [9], Azarova et al. [10], Farzan et al. [11]) which have demonstrated drag reduction for the interaction of a finite heated region with a blunt body. However, in ideal gas simulations, the amount of energy deposited in the flowfield is parameterized by an assumed initial spatial distribution of thermodynamic properties (i.e., translational–rotational temperature and density) and velocity in a finite spatial region. However, these are not the experimental parameters. Instead, the experimental parameters for microwave energy deposition are the microwave frequency and pulse duration, and the electric field distribution and strength. Consequently, ideal gas simulations cannot provide a priori predictions of the interaction of a microwave-generated plasma with an aerodynamic body.

The paper is organized as follows. Section II describes the fully three-dimensional, time-accurate gas dynamic model developed for simulating microwave energy deposition in air. The thermochemistry model includes 23 species and 238 reactions. Section III presents the simulation of the interaction of the microwave-generated plasma with the supersonic flow past a blunt body. The predicted surface centerline pressure is compared with the experiment, and the details of the flowfield structure are described. Section IV summarizes the conclusions. Appendix A provides a detailed description of the thermochemistry model.

II. Model for Microwave Energy Deposition in Air

A fully three-dimensional, time-dependent gas dynamic model for microwave energy deposition in air has been developed incorporating detailed kinetics and thermochemistry. The fluid is assumed inviscid and non-heat-conducting. The relative diffusion of species in the mass conservation equations is neglected. Electron drift and

Table 7 Reactions depending on $E/\mathcal{N}$, part 1

Reaction	A	n	B
Field reactions			
$e + N_2 \rightarrow e + N_2(A^3\Sigma_u^+)$	8.73E − 08	−0.553	398.67
$e + N_2(A^3\Sigma_u^+) \rightarrow e + N_2$	2.22E − 12	1.182	−39.28
$e + N_2 \rightarrow e + N_2(B^3\Pi_g)$	3.63E − 07	−0.775	438.83
$e + N_2(B^3\Pi_g) \rightarrow e + N_2$	4.30E − 11	0.483	−11.33
$e + N_2 \rightarrow e + N_2(a'^1\Sigma_u^-)$	1.66E − 08	−0.474	462.17
$e + N_2(a'^1\Sigma_u^-) \rightarrow e + N_2$	3.99E − 11	0.679	−17.87
$e + N_2 \rightarrow e + N_2(C^3\Pi_u)$	3.38E − 07	−0.621	613.82
$e + N_2(C^3\Pi_u) \rightarrow e + N_2$	1.98E − 10	0.425	10.96
$e + N_2(B^3\Pi_g) \rightarrow e + N_2(C^3\Pi_u)$	1.55E − 05	−1.174	392.06
$e + N_2(C^3\Pi_u) \rightarrow e + N_2(B^3\Pi_g)$	5.60E − 10	0.595	3.70
$e + N_2(C^3\Pi_u) \rightarrow e + e + N_2^+$	4.12E − 05	−0.970	397.86
$e + N_2(A^3\Sigma_u^+) \rightarrow e + N_2(B^3\Pi_g)$	1.90E − 07	−0.053	148.28
$e + N_2(B^3\Pi_g) \rightarrow e + N_2(A^3\Sigma_u^+)$	5.92E − 09	0.317	2.30
Ionization N_2			
$e + N_2(A^3\Sigma_u^+) \rightarrow e + e + N_2^+$	3.30E − 08	−0.130	502.20
$e + N_2(B^3\Pi_g) \rightarrow e + e + N_2^+$	1.59E − 07	−0.320	464.26
$e + N_2(a'^1\Sigma_u^-) \rightarrow e + e + N_2^+$	6.45E − 07	−0.490	436.13
$e + N_2 \rightarrow e + e + N_2^+$	6.33E − 10	0.426	848.82
$e + N_2 \rightarrow e + e + N^+ + N$	2.49E − 06	−1.226	2149.74
N_2 dissociation			
$e + N_2 \rightarrow e + N + N$	7.56E − 10	0.388	662.90
N reactions			
$e + N \rightarrow e + N(^2D)$	1.28E − 04	−1.520	377.60
$e + N(^2D) \rightarrow e + N$	4.85E − 09	0.009	6.22
$e + N \rightarrow e + N(^2P)$	2.29E − 05	−1.432	399.01
$e + N(^2P) \rightarrow e + N$	3.25E − 09	−0.004	9.01
$e + N(^2D) \rightarrow e + N(^2P)$	7.71E − 05	−1.506	397.60
$e + N(^2P) \rightarrow e + N(^2D)$	9.42E − 08	−0.306	13.93
$e + N \rightarrow e + e + N^+$	1.05E − 10	0.627	764.98

Table 8 Reactions depending on $E/\mathcal{N}$, part 2

Reaction	A	n	B
O_2 reactions			
$e + O_2 \rightarrow e + O + O$	3.86E − 06	−1.180	408.08
$e + O_2 \rightarrow e + O + O(^1D)$	1.94E − 06	−0.795	455.44
$e + O_2 \rightarrow e + O + O(^1S)$	6.90E − 11	0.109	481.36
$e + O_2 \rightarrow e + O(^1D) + O(^1S)$	2.93E − 11	0.281	772.18
Ionization O_2			
$e + O_2 \rightarrow e + e + O_2^+$	1.30E − 10	0.649	509.00
$e + O_2 \rightarrow e + e + O^+ + O$	4.50E − 11	0.472	1084.74
$e + O_2 \rightarrow e + O^+ + O^-$	2.03E − 12	0.475	957.51
$e + O_2 \rightarrow O + O^-$	3.93E − 06	−1.818	405.32
O reactions			
$e + O \rightarrow e + O(^1D)$	2.58E − 05	−1.407	364.2
$e + O(^1D) \rightarrow e + O$	2.51E − 09	0.229	13.5
$e + O \rightarrow e + O(^1S)$	1.61E − 06	−1.294	397.4
$e + O(^1S) \rightarrow e + O$	2.34E − 09	0.201	1.1
$e + O \rightarrow e + e + O^+$	5.34E − 09	0.008	727.0
NO reactions			
$e + NO \rightarrow e + e + NO^+$	2.09E − 09	0.282	481.0
$e + NO \rightarrow N + O^-$	2.61E − 06	−1.750	448.6

diffusion are omitted. The Lorentz and Coulomb forces in the momentum equation are also omitted. Radiative phenomena are not included, and the interaction of the incident microwave discharge and the developing streamer discharge are omitted.

The governing equations are as follows:

Mass

$$\frac{\partial \rho_i}{\partial t} + \frac{\partial \rho_i u_j}{\partial x_j} = \dot{\omega}_i \quad \text{for } i = 1, n \tag{1}$$

Momentum

$$\frac{\partial \rho u_i}{\partial t} + \frac{\partial \rho u_i u_j}{\partial x_j} = -\frac{\partial p}{\partial x_i} \quad \text{for } i = 1, 3 \tag{2}$$

Table 9 Heating fractions

Reaction	α_i
$N_2(a'^1\Sigma_u^-) + N \rightarrow N_2 + N(^2P)$	0.480
$N_2(a'^1\Sigma_u^-) + O_2 \rightarrow N_2 + O + O$	0.390
$N_2(A^3\Sigma_u^+) + N \rightarrow N_2 + N(^2P)$	0.270
$N_2(a'^1\Sigma_u^-) + N_2(a'^1\Sigma_u^-) \rightarrow N_2(B^3\Pi_g) + N_2$	0.660
$N_2(A^3\Sigma_u^+) + N_2(B^3\Pi_g) \rightarrow N_2(C^3\Pi_u) + N_2$	0.970
$N_2(A^3\Sigma_u^+) + O_2 \rightarrow N_2 + O + O$	0.360
$N_2(A^3\Sigma_u^+) + O \rightarrow N_2 + O(^1S)$	0.310
$N_2(B^3\Pi_g) + N \rightarrow N_2 + N(^2P)$	0.690
$N_2(B^3\Pi_g) + O_2 \rightarrow N_2 + O + O$	0.550
$N_2(C^3\Pi_u) + N \rightarrow N_2(B^3\Pi_g) + N$	0.080
$N_2(C^3\Pi_u) + N \rightarrow N_2 + N(^2P)$	0.950
$N_2(C^3\Pi_u) + N_2 \rightarrow N_2(a'^1\Sigma_u^-) + N_2$	0.090
$N_2(C^3\Pi_u) + N_2 \rightarrow N_2(B^3\Pi_g) + N_2$	0.930
$N_2(C^3\Pi_u) + O_2 \rightarrow N_2 + O(^1D) + O(^1D)$	0.870
$N_2(C^3\Pi_u) + O_2 \rightarrow N_2 + O + O(^1D)$	0.930
$O(^1D) + O_2 \rightarrow O + O_2$	0.400
$O(^1D) + N_2 \rightarrow O + N_2$	0.400
$O(^1S) + O_2 \rightarrow O_2 + O$	0.700
$N(^2P) + N \rightarrow N(^2D) + N$	1.000
$N(^2P) + O \rightarrow N(^2D) + O$	1.000
$N(^2D) + N_2 \rightarrow N_2 + N$	1.000
$O(^1D) + O \rightarrow O + O$	1.000
$O(^1D) + NO \rightarrow NO + O$	1.000
$O(^1S) + O \rightarrow O + O(^1D)$	1.000
$e + N_2^+ \rightarrow N + N(^2D)$	1.000
$e + N_2^+ \rightarrow N(^2D) + N(^2D)$	1.000
$e + N_2^+ \rightarrow N + N(^2P)$	1.000
$e + NO^+ \rightarrow N + O$	1.000
$e + NO^+ \rightarrow N(^2D) + O$	1.000
$e + O_2^+ \rightarrow O(^1D) + O$	1.000
$e + O_2^+ \rightarrow O(^1D) + O(^1D)$	1.000
$e + O_2^+ \rightarrow O + O$	1.000

Energy

$$\frac{\partial \rho \varepsilon}{\partial t} + \frac{\partial}{\partial x_j}(\rho \varepsilon + p) u_j = \dot{q} \tag{3}$$

Definitions

$$\varepsilon = H - \frac{p}{\rho} \tag{4}$$

$$H = h + \frac{1}{2} u_i u_i \tag{5}$$

$$h = \sum_{i \neq e} Y_i h_i \tag{6}$$

$$h_i = h_{f_i}^o + \int_{T_{\text{ref}}}^{T} c_{p_i} \mathrm{d}T \tag{7}$$

$$p = \mathcal{R} T \sum_{i \neq e} \frac{\rho_i}{M_i} + N_e k T_e \tag{8}$$

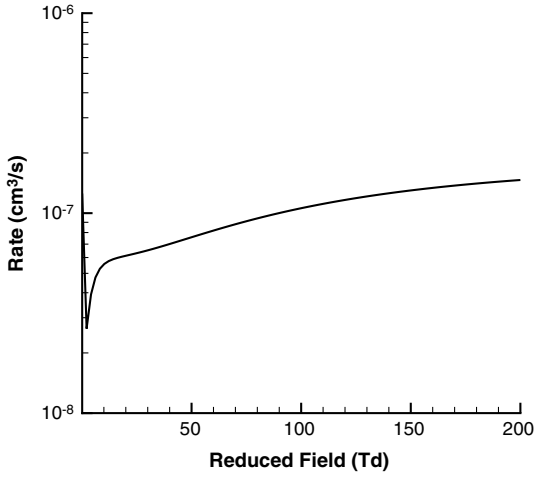

Fig. 4 K_{v_e} **vs** $E/\mathcal{N}|_r$.

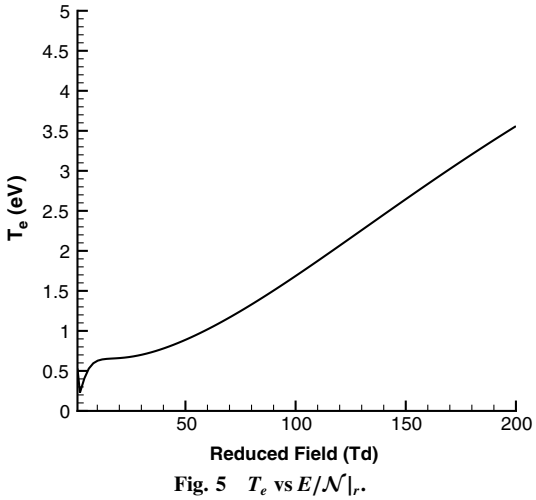

Fig. 5 T_e **vs** $E/\mathcal{N}|_r$.

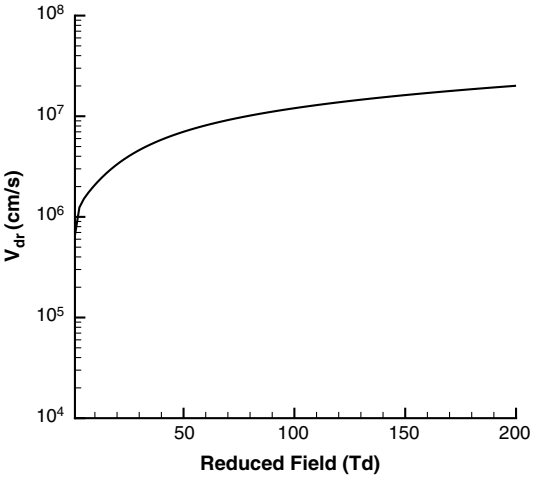

Fig. 6 V_{dr} **vs** $E/\mathcal{N}|_r$.

$$\rho = \sum_{i \neq e} \rho_i \tag{9}$$

Thermochemistry Model

The thermochemistry model [12] incorporates 23 species (e, N_2, O_2, NO, N, O, $N_2(A^3\Sigma_u+)$, $N_2(B^3\Pi_g)$, $N_2(C^3\Pi_u)$, $N_2(a'^1\Sigma_u^-)$, $O(^1D)$, $O(^1S)$, $N(^2D)$, $N(^2P)$, N_2^+, O_2^+, NO^+, N_4^+, N^+, O^+, O_2^-, O^-, and O_3^-) and 238 reactions and is discussed in the Appendix. The reactions are represented as

$$\sum_{i=1}^{n} \nu'_{ik} \mathcal{M}_i \rightarrow \sum_{i=1}^{n} \nu''_{ik} \mathcal{M}_i \quad \text{for } k = 1, m \tag{10}$$

where $\mathcal{M}_i$ represents species i. The rate of production of species $(\text{kg/m}^3 \cdot \text{s})$ is

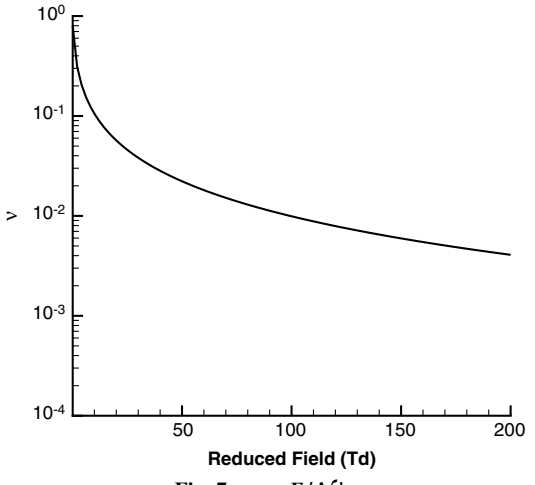

Fig. 7 ν **vs** $E/\mathcal{N}|_r$.

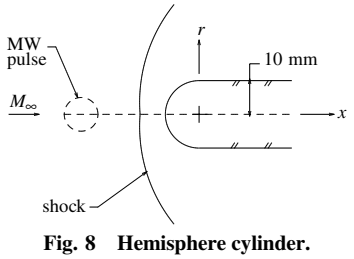

Fig. 8 Hemisphere cylinder.

Table 10 Freestream conditions

Quantity	Value
M_∞	2.1
p_∞, torr	26
T_∞, K	154
D, cm	2.0
N_{N_2}, cm^{-3}	1.287×10^{18}
N_{O_2}, cm^{-3}	3.422×10^{17}
$N_{O_2^+}$, cm^{-3}	3.0×10^4
N_e, cm^{-3}	3.0×10^4

Table 11 Microwave

Quantity	Value
E_o, kV/cm	2.3
λ, cm	3.33
f, GHz	9.0
τ_o, μs	1.20
τ_1, μs	1.21
x_o, cm	−3.5

$$\dot{\omega}_i = \frac{10^6}{\mathcal{A}} M_i \sum_{k=1}^{m} \dot{p}_{i_k} \quad \text{for } i = 1, n \tag{11}$$

$$\dot{p}_{i_k} = (\nu''_{ik} - \nu'_{ik}) K_k \prod_{j=1}^{n} N_j^{\nu'_{jk}} \quad \text{for } i = 1, n; \qquad k = 1, m \tag{12}$$

where N_j is the concentration of species j (cm^{-3}) and $\mathcal{A} = 6.02214 \times 10^{26}$ particles/kg · mol is Avogadro's constant. The reaction coefficients K_k are defined by Khmara et al. [12] according to

$$K_k = AX^n \exp\left(-\frac{B}{X}\right) \tag{13}$$

where X is the local gas temperature T (Kelvin), electron temperature T_e (Kelvin), or reduced field $E/\mathcal{N}|_r$ (Townsend) depending upon the reaction; A, n, and B are constants, and $\mathcal{N}$ is the total concentration (excluding N_e). The units of K_k are

$$\text{units of } K_k = \left(\frac{\text{particles}}{\text{cm}^3}\right)^{1-\sum_{j=1}^{n} \nu'_{jk}} \frac{1}{\text{s}} \tag{14}$$

The reactions and reaction constants are listed in Tables 1–8.

Rate of Gas Heating

The rate of gas heating per unit volume $\dot{q}$ comprises three contributions as discussed in the Appendix. First, the energy lost by electrons in elastic collision with heavy particles (i.e., neutrals and ions) is [13]

$$\dot{q}_{\text{elastic}} = \frac{3}{2} k T_e \delta \nu_e N_e \tag{15}$$

where $\delta = 2m_e/M$, where m_e is the electron mass, M is a representative mass for the neutrals and ions, $\nu_e = \nu_c(1 - \overline{\cos\theta})$ is

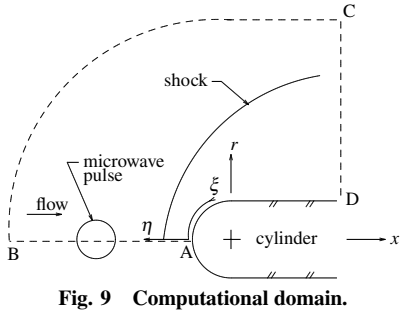

Fig. 9 Computational domain.

Table 12 Details of grids

Quantity	Grid no. 1	Grid no. 2
N_ξ	276	550
N_η	90	180
N_{total}	24,840	99,000
Δr_{min}, cm	4.00×10^{-2}	2.00×10^{-2}
Δr_{max}, cm	4.00×10^{-2}	2.00×10^{-2}
Δs_{min}, cm	1.13×10^{-2}	0.57×10^{-2}
Δs_{max}, cm	5.86×10^{-2}	2.95×10^{-2}
N_p	36	36

the effective collision frequency [see Eq. (22)], and N_e is the electron concentration. The energy lost by electrons in elastic collisions with heavy particles is assumed to be completely transferred into heating of the gas [i.e., increasing the (translational) temperature of the gas].

Second, a fraction of the energy of the reactions is assumed to be completely transferred into heating of the gas

$$\dot{q}_{\text{reactions}} = \sum_{i=1}^{m} \alpha_i \Delta h_i \tag{16}$$

where α_i is the fraction of the rate of change of enthalpy per unit volume Δh_i for reaction i that goes into heating of the gas. The reactions with $\alpha_i \neq 0$ are listed in Table 9, and $\alpha_i = 0$ for all other reactions.

Third, the rotational heating of the gas through microwave energy deposition is given by

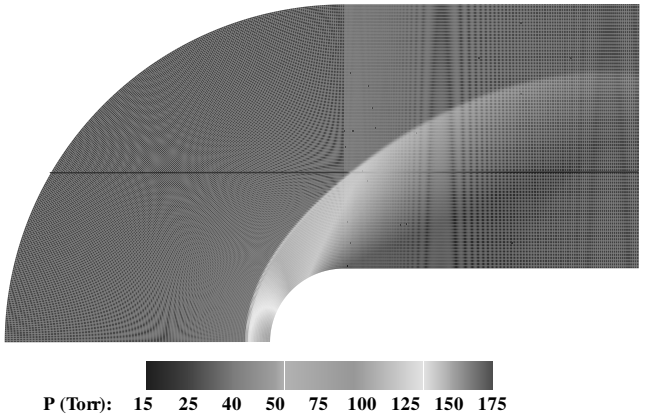

Fig. 10 Pressure contours for steady flow past hemisphere cylinder.

$$\dot{q}_{\text{rotational}} = \nu e \frac{E}{\mathcal{N}}\bigg|_r \mathcal{N} V_{\text{dr}} N_e \tag{17}$$

where ν is the rotational relaxation factor, e is the electron charge, $E/\mathcal{N}|_r$ is the reduced field, $\mathcal{N}$ is the total concentration of species (excluding electrons), and V_{dr} is the electron drift velocity.

Thus, the total energy added per unit volume per unit time is

$$\dot{q} = \frac{3}{2} k T_e \delta \nu_e N_e + \sum_{i=1}^{m} \alpha_i \Delta h_i + \nu e \frac{E}{\mathcal{N}}\bigg|_r \mathcal{N} V_{\text{dr}} N_e \tag{18}$$

Reduced Field and Other Parameters

The reduced field is defined as [12]

$$\frac{E}{\mathcal{N}}\bigg|_r = \frac{E(x_i, t)}{\mathcal{N}} \mu_1 \mu_2 \tag{19}$$

$$\mu_1 = \left[1 + \left(q \frac{N_e}{N_e^{\text{crit}}}\right)\right]^{-1/2} \tag{20}$$

$$\mu_2 = \frac{\nu_e}{\sqrt{\nu_e^2 + \omega^2}} \tag{21}$$

where q is the depolarization factor, N_e^{crit} is the critical electron concentration, ω is the microwave angular frequency (rad per second), and ν_e is the effective frequency of electron collisions with reagents given by

$$\nu_e = \mathcal{N} K_{\nu_e} \tag{22}$$

where

$$K_{\nu_e} = \exp\left[\sum_{i=0}^{9} a_i \left(\log_e \frac{E}{\mathcal{N}}\bigg|_r\right)^i\right] \tag{23}$$

where ν_e is in s^{-1}, $E/\mathcal{N}|_r$ is in Townsend, $\mathcal{N}$ is the concentration in cm^{-3} (neglecting electrons) and a_i are specified constants. Equation (19) is an implicit equation for $E/\mathcal{N}|_r$ and is solved by Newton's method. The expression for K_{ν_e} is shown in Fig. 4.

The electron temperature T_e is given by

$$T_e = \exp\left[\sum_{i=0}^{9} b_i \left(\log_e \frac{E}{\mathcal{N}}\bigg|_r\right)^i\right] \tag{24}$$

where T_e is in electron volts, $E/\mathcal{N}|_r$ is in Townsend, and b_i are specified constants. The expression is shown in Fig. 5. Electrons are assumed to thermalize instantaneously ($T_e = T$) when $E = 0$.

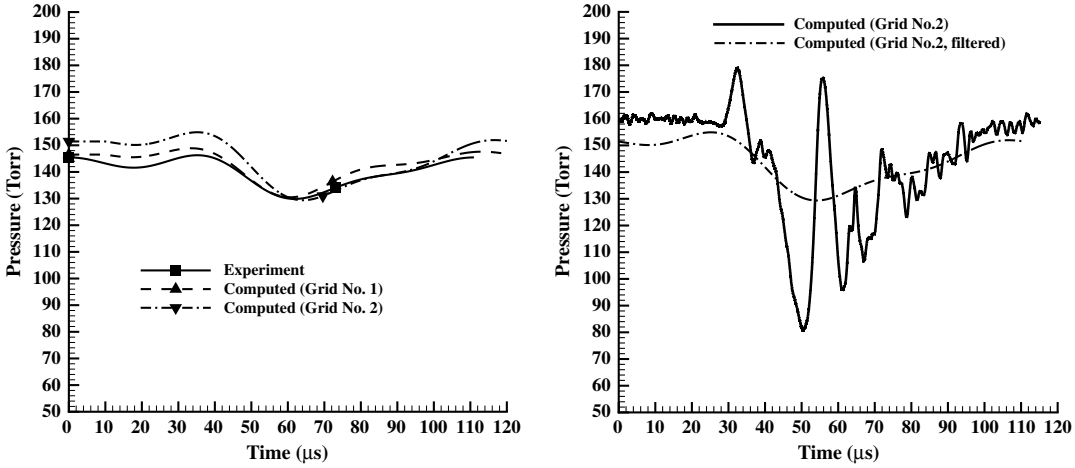

a) Computed and experimental pressure **b) Computed and filtered pressure (Grid No. 2)**

Fig. 11 Computed and experimental pressure on hemisphere-cylinder centerline.

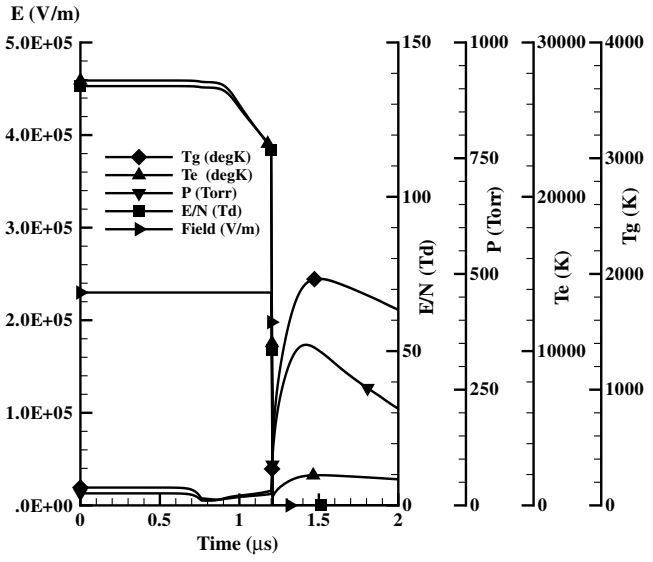

a) p, T, T_e *vs t*

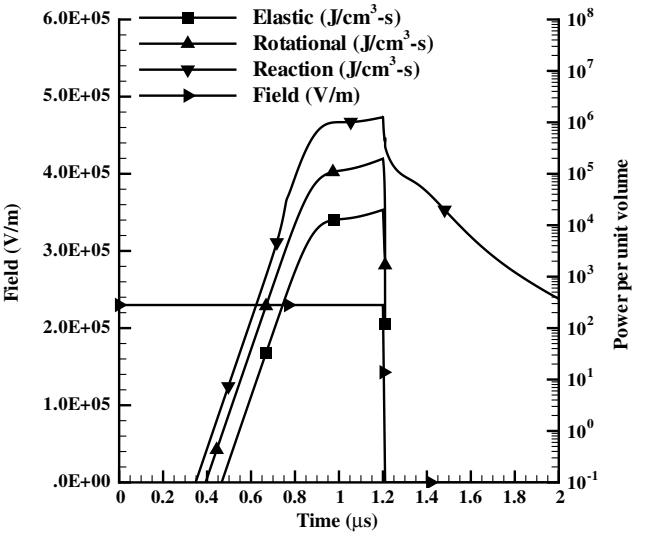

b) Heating terms

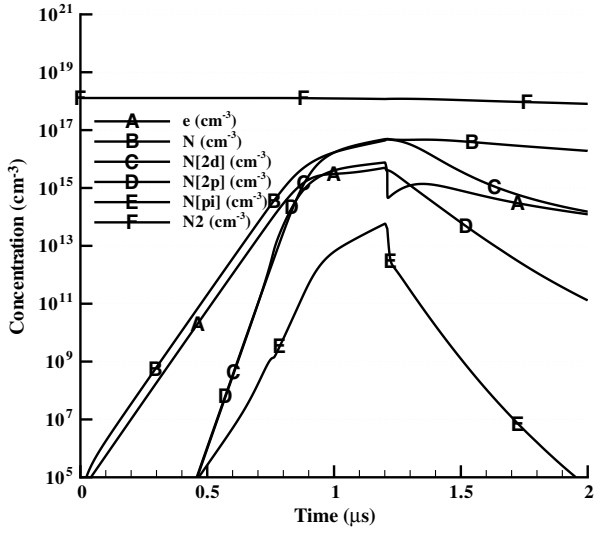

c)

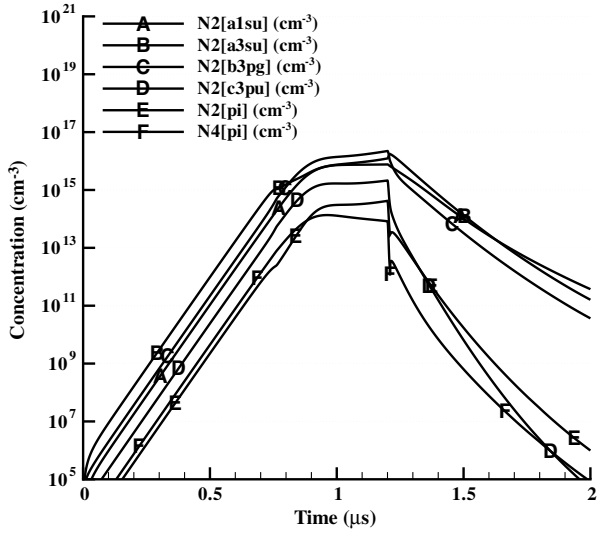

d)

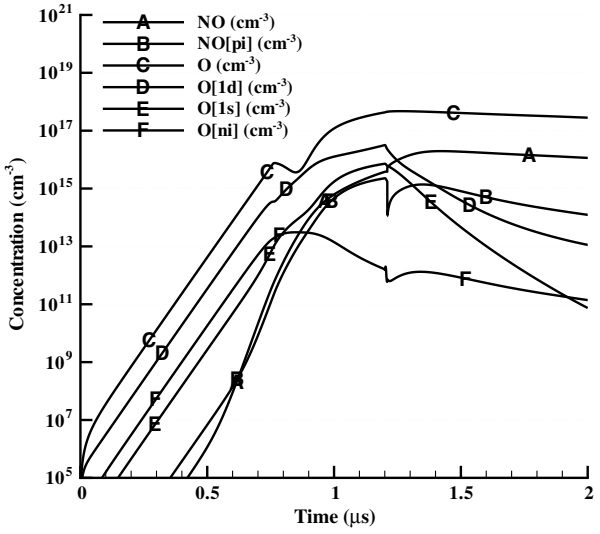

e)

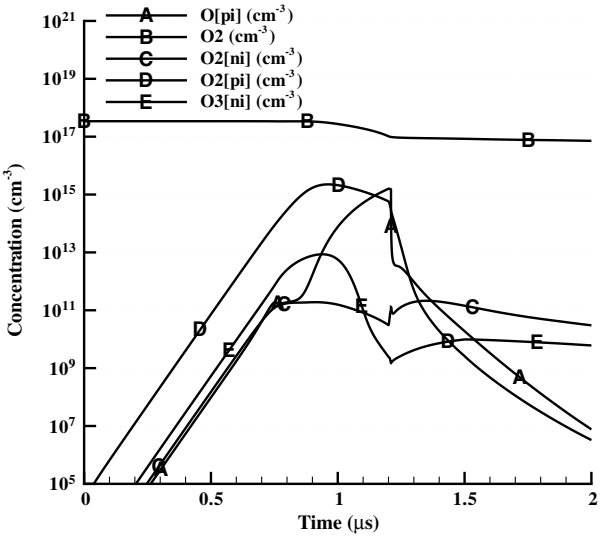

f)

Fig. 12 Properties at center of plasma.

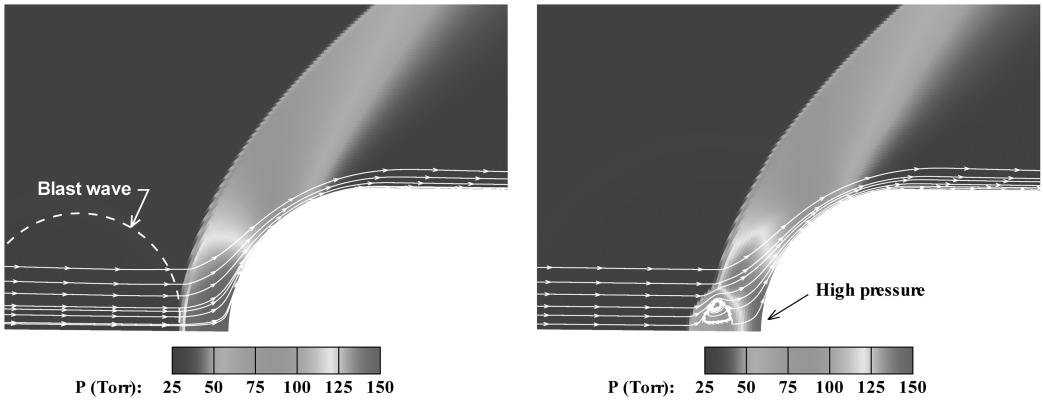

a) $t = 25\ \mu$s b) $t = 42\ \mu$s

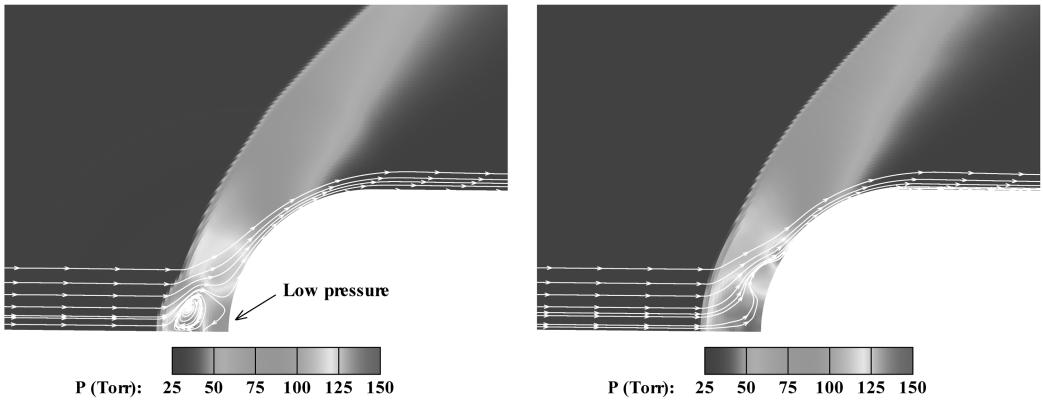

c) $t = 50\ \mu$s d) $t = 75\ \mu$s

Fig. 13 p, torr.

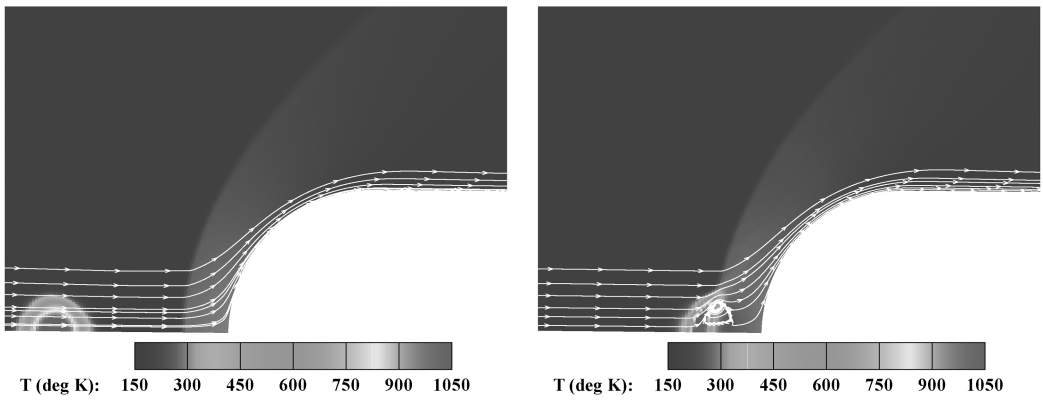

a) $t = 25\ \mu$s b) $t = 42\ \mu$s

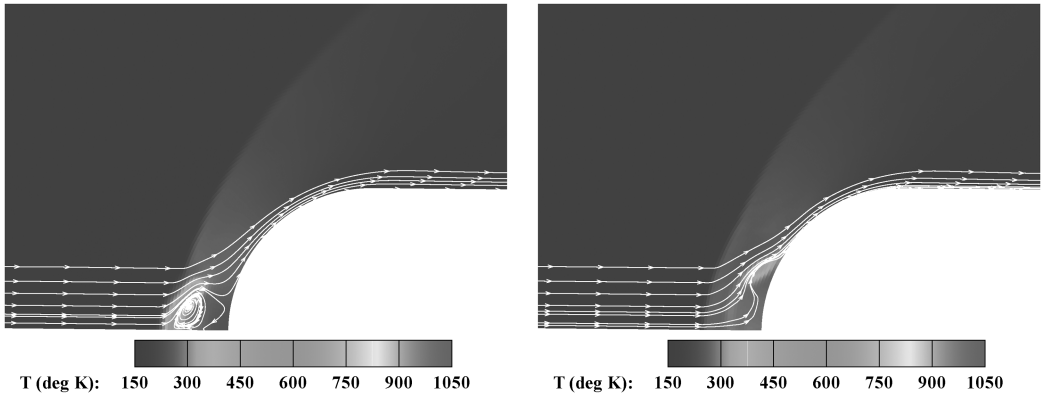

c) $t = 50\ \mu$s d) $t = 75\ \mu$s

Fig. 14 T, K.

The drift velocity $V_{\rm dr}$ is given by

$$V_{\rm dr} = \exp\left[\sum_{i=0}^{9} c_i \left(\log_e \frac{E}{\mathcal{N}}\bigg|_r\right)^i\right] \tag{25}$$

where $V_{\rm dr}$ is in centimeters per second, $E/\mathcal{N}|_r$ is in Townsend, and c_i are specified constants. The expression is shown in Fig. 6.

The rotational relaxation factor ν is given by

$$\nu = d_o \left(\frac{E}{N}\bigg|_r\right)^{d_1} \exp\left(-d_2 \Big/ \frac{E}{N}\bigg|_r\right) \tag{26}$$

where ν is dimensionless, $E/\mathcal{N}|_r$ is in Townsend, and d_i are specified constants. The expression is shown in Fig. 7.

The thermochemistry model was validated by comparison with experimental data for microwave discharge in quiescent air at 70 torr and an initial gas temperature $T_g = 200$ K. The model accurately predicted the final gas temperature within 10 K [14].

Electric Field

The electric field is given by

$$E = \begin{cases} E_o f(t) \cos k_E(x - x_o) \cos k_E r & k_E r \le \frac{1}{2}\pi \text{ and} \\ & k_E|x - x_o| \le \frac{1}{2}\pi \\ 0 & \text{else} \end{cases} \tag{27}$$

where $k_E = 2\pi/\lambda$, λ is the free-space wavelength of the microwave, r is the cylindrical radius, and $f(t)$ is the dimensionless temporal behavior defined by

$$f(t) = \begin{cases} 1 & 0 < t < \tau_o \\ 1 - (t - \tau_o)/(\tau_1 - \tau_o) & \tau_o < t < \tau_1 \\ 0 & t > \tau_1 \end{cases} \tag{28}$$

The spatial form of the electric field is based upon the experimental measurements of Kolesnichenko et al. [15] wherein the electric field for a single microwave-generated plasmoid has a spatial length scale approximately equal to $\lambda/2$. Note that the electric field decreases linearly in time from $t = \tau_o$ to $t = \tau_1$. The center of the electric field is located at $(x, r) = (x_o, 0)$.

The governing equations are solved using a cell-centered structured multiblock code written in C + + by the first author. The inviscid fluxes are discretized using Roe's method extended for multiple species and including a compatibility condition for determination of the static pressure [16]. Temporal integration is performed using a second-order accurate semi-implicit Runge–Kutta method [17]. The code is parallelized using message passing interface [18] and runs on an AMD-64-based cluster under Debian Linux.

III. Interaction of Microwave-Generated Plasma with a Hemisphere Cylinder

A. Configuration

The gas dynamic code has been applied to the simulation of the interaction of a microwave-generated plasma with the flow past a hemisphere cylinder. The flow configuration is shown in Fig. 8. The microwave pulse is focused at a distance x_o upstream of the center of curvature of the hemisphere. The freestream conditions are shown in Table 10 and the microwave parameters in Table 11. The freestream species concentrations for N_2 and O_2 correspond to standard air at the specified static pressure and temperature. A small freestream concentration of electrons N_e and molecular oxygen ions $N_{O_2^+}$ were included. The freestream concentration of all other species (besides N_2, O_2, O_2^+, and electrons) is set to zero. The depolarization factor q was set to zero to approximate the formation of microwave filaments at the core of the discharge.

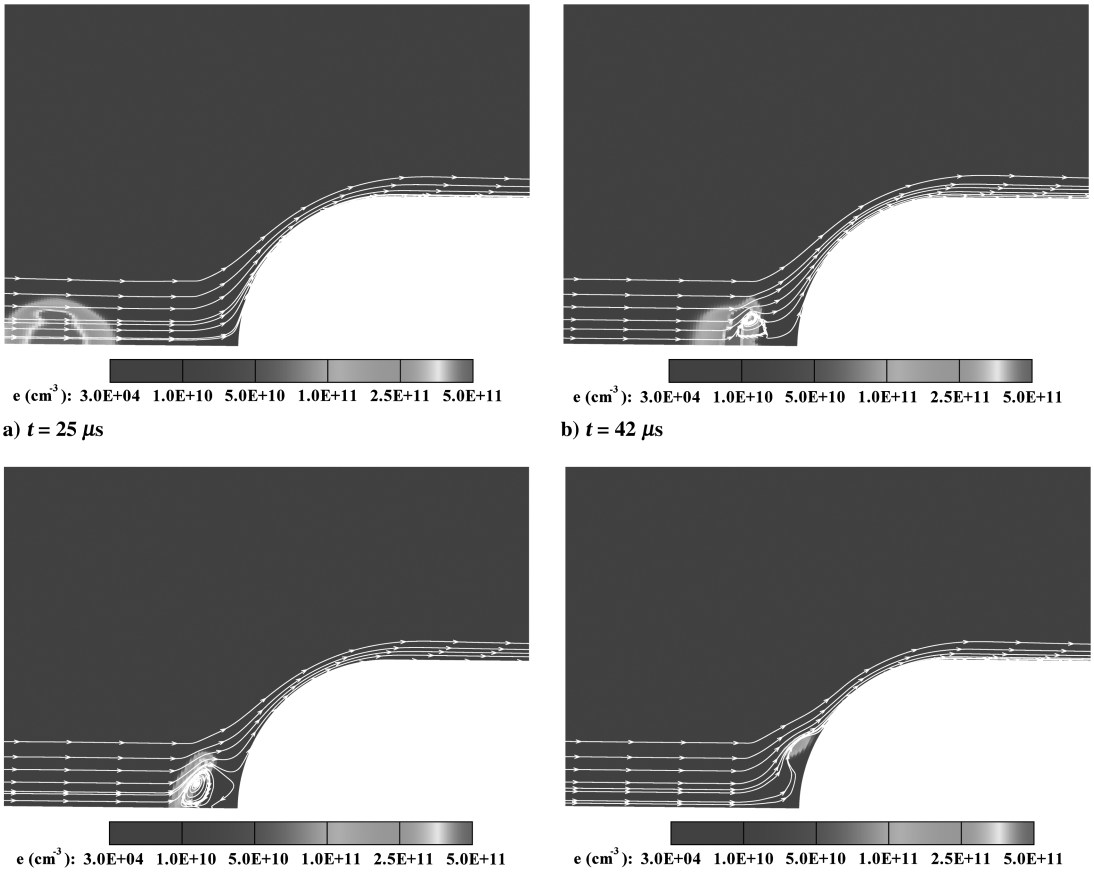

Fig. 15 N_e, cm^{-3}.

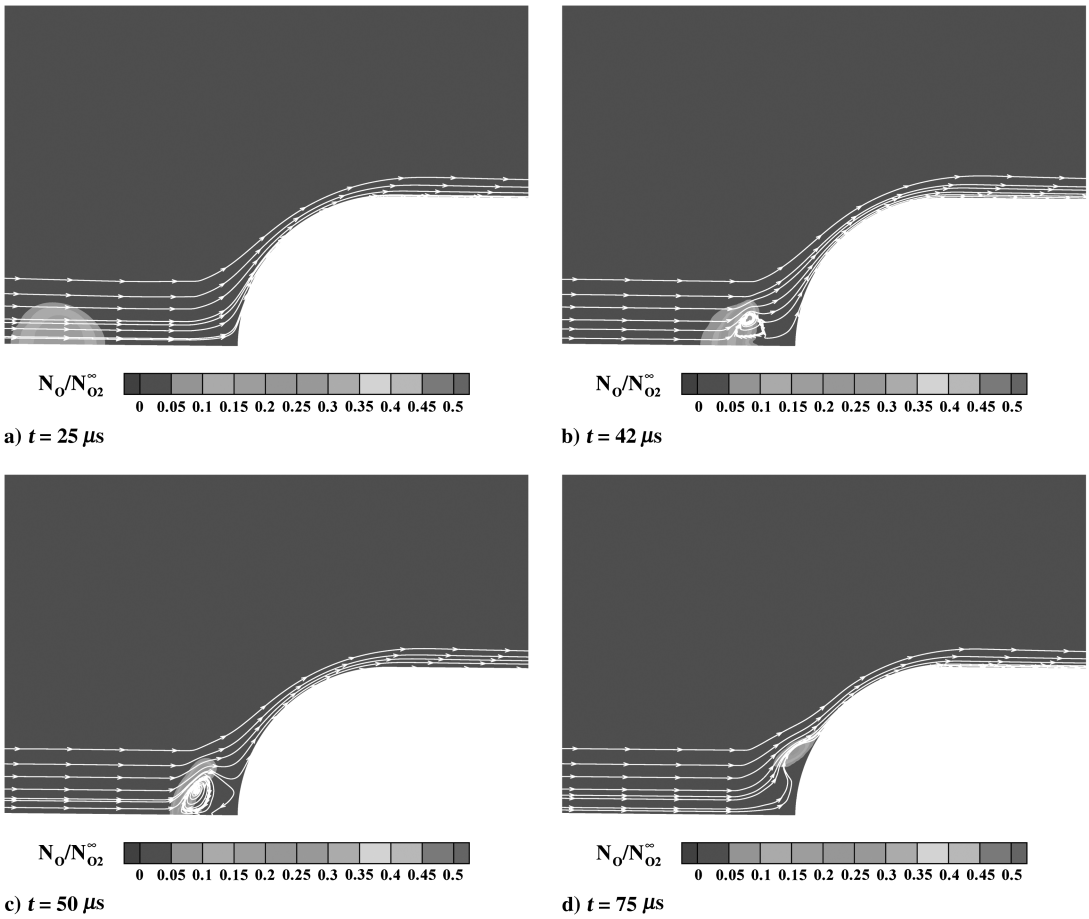

Fig. 16 $N_O/N_{O_2}^{\infty}$.

B. Details of Computations

The computational domain ABCD is illustrated in Fig. 9. Two separate computations were performed to assess the effect of grid refinement on the flowfield. Details of the grids are listed in Table 12. The number of cells N_ξ and N_η in the ξ and η directions, respectively, are indicated, together with the total number of cells N_{total} in the computational domain. The grid spacing Δr in the η direction is uniform and equal to $0.02D$ and $0.01D$ for grid numbers 1 and 2, respectively. The minimum grid spacing Δs in the ξ direction on the hemisphere cylinder is $0.005691D$ and $0.002856D$ for grid numbers 1 and 2, respectively; this enabled an ξ spacing Δs which is approximately equal to the η spacing Δr in the vicinity of the undisturbed shock wave. The number of processors $N_p = 36$. Axis boundary conditions are applied on the symmetry axis AB. Freestream conditions are imposed on the outer boundary BC, and zero gradient conditions at the outflow boundary CD. On the hemisphere-cylinder surface AD, tangential (slip) boundary conditions are applied and the normal derivative of all species is set to zero. The semi-implicit Runge–Kutta algorithm is used in the initial stages of the computation due to the rapid increase in species concentrations and gas temperature in the region of the microwave beam during the microwave pulse. After a few microseconds of physical time, the temporal algorithm is switched to an explicit Runge–Kutta scheme.

C. Initial Conditions

The initial condition for the microwave pulse is the converged solution for flow past the body at the freestream conditions shown in Table 10. The computed static pressure contours for the hemisphere cylinder are shown in Fig. 10. The computed surface pressure on the centerline agrees with the theoretical stagnation pressure downstream of the normal shock to within 0.3%.

D. Comparison with Experiment

The computed and experimental surface pressure vs time on the centerline of the body surface for the hemisphere cylinder are shown in Fig. 11a. There was no analog or digital filtering of the signal from the Kulite pressure transducer. The manufacturer[††] recommends that the transducer signal be filtered at one-fifth of the natural frequency of the transducer. The natural frequency of the experimental pressure transducer is 150 kHz, and therefore the computed and experimental surface pressure was filtered by multiplying the Fourier coefficients of the surface pressure time series by a top-hat filter with cutoff at 30 kHz. The time point of initial pressure decrease was matched between the computation and experiment to account for the uncertainty in the location of the microwave pulse in the experiment. This resulted in a $+10\ \mu$s shift in the computed pressure. The agreement between the computed and experimental surface pressure is good. The effect of the filtering on the computed centerline pressure for grid number 2 is shown in Fig. 11b. The filtering significantly reduces the magnitude of the computed pressure drop associated with the interaction of the microwave-generated plasma and the hemisphere cylinder.

E. Initial Behavior of Plasma

The development of the pressure p, temperature T, and electron temperature T_e at the center of the discharge is shown in Fig. 12a.[‡‡] Also shown is the imposed electric field $E_o f(t)$ and reduced field $E/\mathcal{N}$ at the center. The pressure reaches a maximum value of 346 torr at $t = 1.4\ \mu$s, and the gas temperature reaches a maximum of 1958 K at $t = 1.4\ \mu$s. The maximum reduced field is 135 Townsend (Td). The contributions to the gas heating q_{elastic}, $q_{\text{rotational}}$, and $q_{\text{reactions}}$ at

[††]Technology: Reference Library, pp. 3-7, 3-8, http://www.kulite.com/techinfo.asp.

[‡‡]Hereafter, all results are shown for grid number 2.

the center of the discharge are shown in Fig. 12b. The most significant contribution is $q_{\text{reactions}}$ which reaches a maximum value of 1.25 MW/cm^3 at $t = 1.2$ μs. The corresponding maximum values for $q_{\text{rotational}}$ and q_{elastic} are 0.19 MW/cm^3 and 0.019 MW/cm^3. Note that the rotational relaxation factor ν is on the order of 10^{-2} for a reduced field of 100 Td, thereby accounting for the low level of rotational heating. The rotational heating term becomes zero at the termination of the pulse because the electric field vanishes. Because the collision frequency ν_e is an assumed function of the reduced field from Eq. (23), the elastic heating also goes to zero when the electric field vanishes. Overall, the principal contribution to the gas heating is due to the thermochemical reactions (i.e., the collisional quenching of excited particles and electron-ion recombinations as discussed in the Appendix).

The kinetics of the plasma formation are illustrated in Figs. 12c–12f, which displays the evolution of the concentration (cm^{-3}) of all species at the center of the plasma for $t = 0$ to $t = 2$ μs. Figure 12c indicates a modest dissociation of N_2 with a peak value of N equal to 3.6% of the freestream N_2 concentration. The concentration of the electronically excited states of nitrogen $N(^2D)$, $N(^2P)$, $N_2(a'^1\Sigma_u^-)$, $N_2(A^3\Sigma_u+)$, $N_2(B^3\Pi_g)$, $N_2(C^3\Pi_u)$ do not exceed $4 \cdot 10^{16}$ cm^{-3} (i.e., 3.1% of the freestream N_2 concentration) and rapidly decay (Figs. 12c and 12d). The peak concentration of the excited states of oxygen $O(^1D)$ and $O(^1S)$ are 9.2 and 2.1% of the freestream concentration of O_2, respectively, (Fig. 12e). A substantial dissociation of molecular oxygen occurs with peak concentration of atomic oxygen O equal to 1.38 times the freestream concentration of O_2. The concentration of atomic oxygen remains significant throughout the interaction. The NO concentration reaches a peak value equal to 1.5% of the freestream concentration of N_2 and decays slowly. The concentration of the oxygen ions O^+, O^-, O_2^+, O_2^-, and O_3^-, nitrogen ions N_2^+, N_4^+, N^+, and NO^+ remains low throughout at levels typically below 10^{15} cm^{-3}.

F. Flowfield Structure

The interaction of the microwave-generated plasma with the shock structure of the hemisphere cylinder is shown[§§] in Figs. 13–16. The static pressure contours (Figs. 13a–13d) and static temperature contours (Figs. 14a–14d) display the interaction of the plasma with the shock structure of the blunt body. At $t = 25$ μs, the blast wave (identified by the dotted line in Fig. 13a) has reached the blunt body shock. The plasma is upstream of the shock (Fig. 14a) with a temperature exceeding 1000 K. At $t = 42$ μs, the plasma has reached the blunt body shock (Figs. 13b and 14b). Two significant flow features are evident, namely, 1) the blunt body shock has lensed upstream (forward), and 2) a recirculation region has formed, thereby momentarily streamlining the blunt body. Both of these phenomena have been observed in ideal gas simulations (see, for example, Georgievsky et al. [19]). The recirculation region persists for more than 70 μs as the plasma is convected past the hemisphere (Figs. 13c and 13d).

The evolution of the electron concentration N_e (cm^{-3}) is displayed in Figs. 15a–15d. At the moment the blast wave reaches the blunt body shock ($t = 25$ μs), the peak electron concentration in the plasma is 6.7×10^{11} cm^{-3}. A small increase occurs due to the compression associated with the interaction of the plasma with the blunt body shock (Fig. 15b) where the peak concentration reaches 7.4×10^{11} cm^{-3}. Thereafter, the electron concentration decays slowly with peak value of 2.1×10^{11} cm^{-3} at $t = 75$ μs (Fig. 15d).

The evolution of the ratio of atomic oxygen O concentration to the freestream molecular oxygen O_2 concentration is displayed in Figs. 16a–16d. At $t = 25$ μs, the peak value of the ratio is 0.17. The compression of the plasma associated with its interaction with the blunt body shock increases the peak value of the ratio to 0.32 and later decays to 0.22 at $t = 75$ μs. It is evident that the concentration of atomic oxygen O remains at a significant level throughout the interaction of the plasma with the blunt body shock.

[§§]Note that the times shown are not shifted. To compare with the surface pressure on the centerline in Fig. 11, add 10 μs to the times shown in Figs. 13–16.

IV. Conclusions

A fully three-dimensional, time-accurate gas dynamic code has been developed for simulating microwave energy deposition in air and the interaction of the microwave-generated plasma with the supersonic flow past a blunt body. The thermochemistry model includes 23 species and 238 reactions. The code is written in C++ and parallelized using message passing interface. The code is applied to the simulation of microwave energy deposition in supersonic flow past a hemisphere cylinder. The computed centerline pressure is compared with the experiment and displays close agreement. The kinetic history of the species within the plasma is discussed. The interaction of the plasma with the blunt body shock is described. Significant nonequilibrium effects are observed throughout the interaction; in particular, the level of atomic oxygen remains high through the interaction of the plasma with the blunt body.

Appendix: Thermochemistry Model

The mechanism of energy transfer from the microwave electric field to the gas is illustrated in Fig. A1. The electric field accelerates the electrons (joule heating) which undergo collisions with the heavy particles. The elastic collisions between electrons and heavy particles result in a very small increase in the kinetic energy of heavy particles because the ratio of the electron mass to the typical mass of the heavy particles is on the order of 10^{-5} (see Fig. 12b). The increase in the (translational) temperature of the gas is given by $\dot{q}_{\text{elastic}}$ in Eq. (15).

The inelastic collisions between electrons and heavy particles result in a variety of modes of energy transfer, namely, 1) rotational excitation, 2) vibrational excitation, 3) excitation of electronic states, 4) dissociations, and 5) ionization. There are three principal kinetic channels for the energy transfer from these modes to the kinetic energy of the heavy particles, namely, 1) rotational relaxation, 2) collisional quenching of excited particles, and 3) electron-ion recombination. The relation between these channels depends principally on the energy deposition (electron concentration).

The relaxation of the rotationally excited molecules is represented in the model by $q_{\text{rotational}}$ in Eq. (17). Rotational relaxation is the mechanism of "direct" gas heating whereby a fraction of energy input into the discharge, which causes rotational excitation of N_2 and O_2, relaxes within ten intermolecular collisions to the kinetic energy of the molecules. The rotational relaxation factor ν in Eq. (17) decreases with increased reduced field as indicated in Fig. 7.

During collisional quenching of electron-excited atoms and molecules, the energy defect of reaction is distributed between internal and kinetic energies of reaction products. In most cases, the

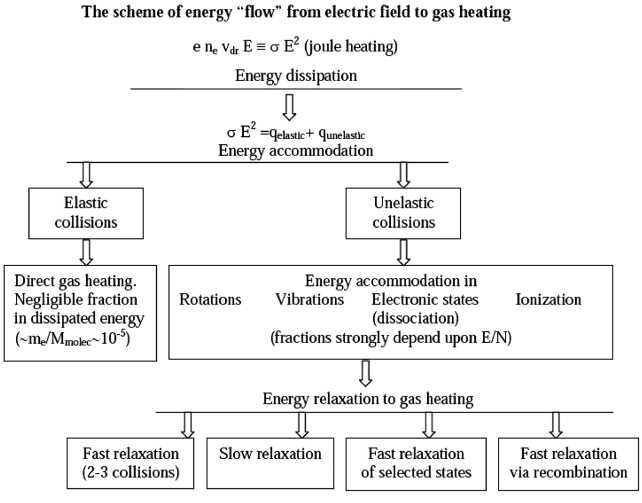

Fig. A1 Channels of gas heating.

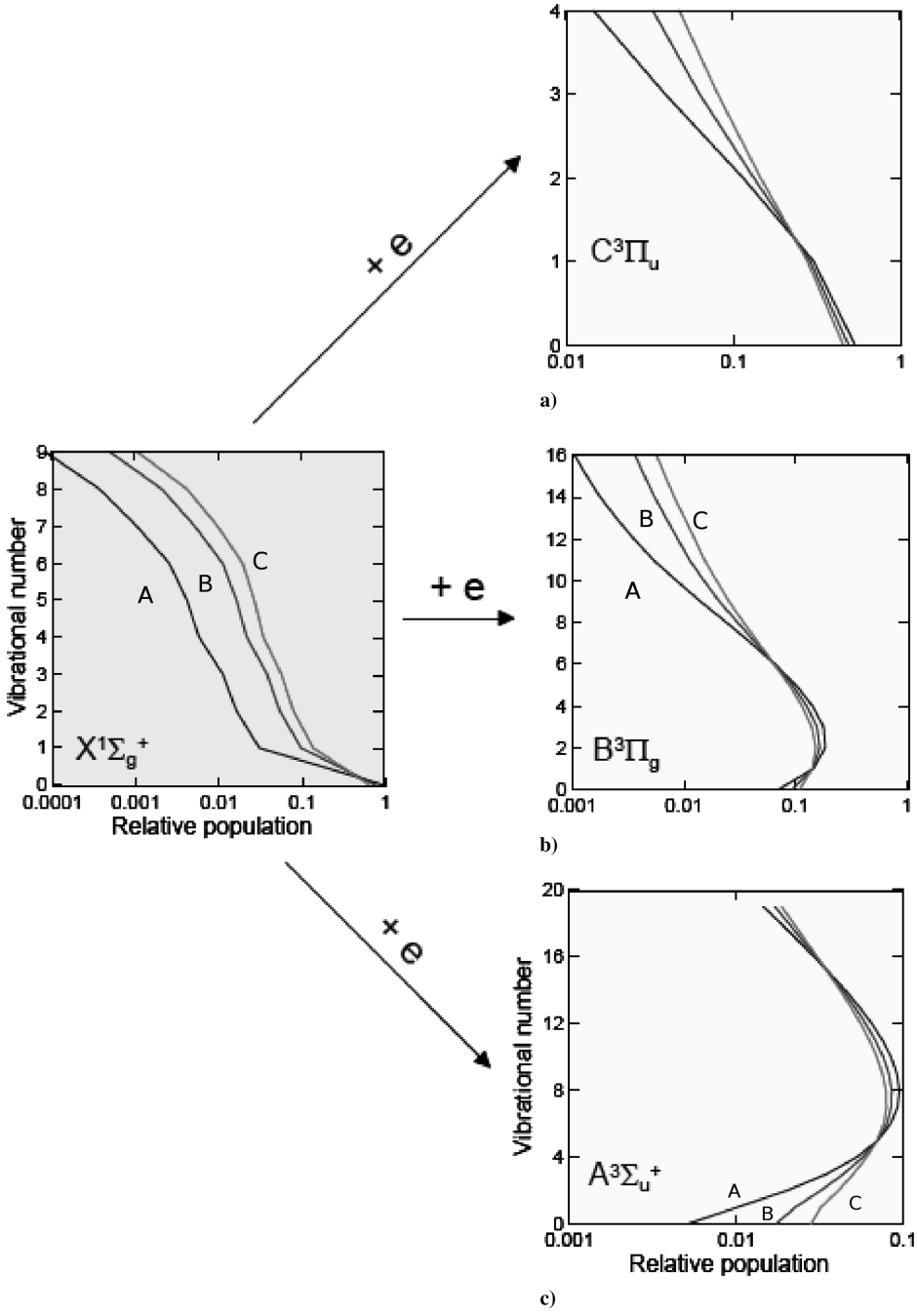

Fig. A2 Vibrational distribution functions of first N_2 triplets during its excitation from the ground state by electron impact. $E/N = 100$ Td, energy deposition ($J/cm^3 \cdot atm$): 0.2 (A), 0.8 (B), 1.4 (C).

fraction of such distribution is unknown with the exception of the family of reactions

$$M^* + O_2 \rightarrow M + O + O \tag{A1}$$

$$M^* + N \rightarrow M + N \tag{A2}$$

where $M^* = N_2(A^3\Sigma_u^+)$, $N_2(B^3\Pi_g)$, $N_2(a'^1\Sigma_u^-)$, $N_2(C^3\Pi_u)$. In these cases, permission or prohibition of the reaction on the basis of energy arguments and permission or prohibition of $M^* \rightarrow M$ vibrational transitions allows the determination of the heat effect of reactions.

The relative population of ν' vibrational levels of the M^* state at the moment of collision is

$$\tilde{N}_{\nu'} = \sum_{\nu} q_{\nu\nu'} \tilde{N}_{\nu} \tag{A3}$$

where $\tilde{N}_{\nu}$ is the relative population of ν vibrational levels of the ground electronic state, and $q_{\nu\nu'}$ is the Franck–Condon factor for $\nu \rightarrow \nu'$ transition. This expression corresponds to the case when the M^* state is populated by electron impact from the ground state and the vibrational distribution function of the M^* state is substantially nonequilibrium. The typical distributions of vibrational states [14] for nitrogen triplets are shown in Fig. A2. As a result of a collision, the M^* state transits to ν'' levels of the M state with the possibilities corresponding to $q_{\nu\nu'}$ (the Franck–Condon factors of the $\nu \rightarrow \nu'$ transitions). At this energy change, $E_{\nu'\nu''}$ equals the difference between (M^*, ν') and (M, ν'') energies. The transitions with $E_{\nu'\nu''} < E_{\text{diss}}$ (where E_{diss} is the dissociation energy of the second colliding particle) are forbidden. The expression $q_{\nu'\nu''}(E_{\nu'\nu''} - E_{\text{diss}})$ determines the heat effect of the permitted $(M^*, \nu') \rightarrow (M, \nu'')$ transition. The total heat effect of reaction E_r is the sum over the heat effects of the individual vibrational transitions. This method is described in Popov [20] and was used in our simulations. Our calculations show

that E_r depends weakly on the vibrational distribution of the ground electronic state (within 10–20%). The accepted heat effects of the reactions (A1) and (A2) are listed in Table A1. Reactions similar to Eq. (A2) but with the participation of oxygen atoms were not taken into account as a heating channel because these reactions mainly lead to N_2 oxidation (NO + N) with an unknown heat effect.

Another family of energy transfer heating reactions is

$$O[^1D] + M \rightarrow O + M^* \tag{A4}$$

where $M = N_2, O_2, M^* = N_2, O_2, O_2(a^1\Delta_g), O_2(b^1\Sigma_g^+)$. According to Slanger and Black [21], the brutto heat effect of the $O(^1D)$ collisional quenching is 70% of excitation energy, that is, 1.38 eV. This value was used in the model.

Dissociative recombination of electrons with diatomic ions (N_2^+, O_2^+, NO^+) is one more class of plasma heating reactions. There are direct measurements of kinetic and internal energy of reaction products [22–25]. The accepted values of the model heat effects of these reactions are shown in Table A2. This model was used for the kinetic description of the microwave halo and filament [26].

The present model is a simplification of an earlier kinetic model [26] which included 721 reactions among 44 charged, neutral, and excited species, and was validated by comparison of calculated second positive system of molecular nitrogen emission dynamics and plasma heating with experimental measurements [26]. For modeling of the airflow interaction with microwave discharge plasmoids, however, the earlier kinetic model is overly complicated. The main aim of plasma kinetic modeling in a gas dynamic problem is the proper description of the gas heating. In the context of the kinetic mechanism, the scheme of fast plasma heating exists. It includes the following heating channels, leading to the filament formation during heat instability development: 1) rotational relaxation of N_2 and O_2 (at the beginning stage), 2) collisional quenching of electronically excited atoms and molecules, such as $N_2(A^3\Sigma_u^+)$, $N_2(B^3\Pi_g)$, $N_2(C^3\Pi_u)$, $N_2(a'^1\Sigma_u^-)$, $O(^1D)$, $O(^1S)$, $N(^2D)$, $N(^2P)$ (at the beginning stage), and 3) electron-ions dissociative recombination $e + N_2^+$, O_2^+, NO^+ (at the final stage). It was therefore necessary to reduce the size of the kinetic model while maintaining an adequate description of the dynamics of charged and excited particles production. Because the time of plasma development from the initial electron concentration is on the order of 1 μs, it is reasonable to neglect tertiary molecules (NO_2, N_2O, O_3, etc.). The reactions of high-temperature collisional dissociation of main species and their ions $M + N_2, O_2 \rightarrow M +$ products become negligible because the main channel of dissociation occurs by electron impact and high-temperature mechanism "switch on" at the final stage of plasma formation when the medium becomes the mixture of N_2-N-O. Three body reactions of neutral atoms recombination are important during a high degree of dissociation, that is, at the final stage; however, at this stage, the medium is rather hot and such reactions occur slowly because the rate constants of three body reactions decrease with increase in temperature. These aforementioned assumptions permit the reduction of the complete kinetic mechanism to the present model with 23 species and 238 reactions.

Table A1 Heat effects of reactions

M^*	Allowed M	Heat effect, eV
	$M^* + O_2 \rightarrow M + O + O$	
$A^3\Sigma_u^+$	$X^1\Sigma_g^+$	0.29
$B^3\Pi_g$	$X^1\Sigma_g^+$	1.23
$a'^1\Sigma_u^-$	$X^1\Sigma_g^+$	1.28
$C^3\Pi_u$	$X^1\Sigma_g^+$	3.58, 1.79[a]
	$M^* + N \rightarrow M + N(^2P)$	
$A^3\Sigma_u^+$	$X^1\Sigma_g^+$	0.61
$B^3\Pi_g$	$X^1\Sigma_g^+$	2.38
$a'^1\Sigma_u^-$	$X^1\Sigma_g^+$	2.16

[a]One or both oxygen atoms in ^1D state, correspondingly.

Table A2 Heat effects of dissociative recombination reactions

Products	Heat effect, eV
$e + N_2^+$	
$N[^2D] + N$	1.44
$N[^2P] + N$	0.20
$N[^2D] + N[^2D]$	0.51
$e + O_2^+$	
$O[^1D] + O$	3.73
$O[^1D] + O[^1D]$	0.60
$O[^1D] + O[^1S]$	0.04
$e + NO^+$	
$N + O$	1.38
$N[^2D] + O$	0.19

Acknowledgments

This research is supported by the U.S. Air Force Office of Scientific Research under Grant FA9550-07-1-0228 and by the European Office of Aerospace Research and Development under Grant ISTC 047003. Both grants are managed by John Schmisseur. The support of U.S. Air Force Office of Scientific Research European Office of Aerospace Research and Development (Surya Surampudi) is gratefully acknowledged.

References

[1] Cattafesta, L., III, Song, Q., Williams, D., Rowley, C., and Alvi, F., "Active Control of Flow-Induced Cavity Oscillations," *Progress in Aerospace Sciences*, Vol. 44, Nos. 7–8, Oct.–Nov. 2008, pp. 479–502. doi:10.1016/j.paerosci.2008.07.002

[2] Zheltovodov, A., "Development of the Studies on Energy Deposition for Application to the Problems of Supersonic Aerodynamics," Preprint 10-2002, Inst. of Theoretical and Applied Mechanics, Novosibirsk, Russia, 2002, p. 43.

[3] Knight, D., Kuchinskiy, V., Kuranov, A., and Sheikin, E., "Survey of Aerodynamic Flow Control at High Speed Using Energy Addition," AIAA Paper 2003-0525, Jan. 2003.

[4] Fomin, V., Tretyakov, P., and Taran, J.-P., "Flow Control Using Various Plasma and Aerodynamic Approaches (Short Review)," *Aerospace Science and Technology*, Vol. 8, No. 5, July 2004, pp. 411–421. doi:10.1016/j.ast.2004.01.005

[5] Knight, D., "Survey of Aerodynamic Drag Reduction at High Speed by Energy Deposition," *Journal of Propulsion and Power*, Vol. 24, No. 6, Nov.–Dec. 2008, pp. 1153–1167. doi:10.2514/1.24595

[6] Lashkov, I., Mashek, I., Anisimov, Y., Ivanov, V., Kolesnichenko, Y., Ryvkin, M., and Gorynya, A., "Gas Dynamic Effect of Microwave Discharge on Supersonic Cone-Shaped Bodies," AIAA Paper 2004-0671, Jan. 2004.

[7] Kolesnichenko, Y., Azarova, O., Brovkin, V., Khmara, D., Lashkov, V., Mashek, I., and Rivkin, M., "Basics in Beamed MW Energy Deposition for Flow/Flight Control," AIAA Paper 2004-0669, Jan. 2004.

[8] Kolesnichenko, Y., "Microwave discharge in free space," *Thematic Workshop on Fundamentals of Aerodynamic Flow and Combustion Control by Plasmas*, European Conference for Aerospace Sciences, May 2007.

[9] Georgievsky, P., and Levin, V., "Unsteady Interaction of a Sphere with Atmospheric Temperature Inhomogeneity at Supersonic Speed," *Mekhanika Zhidkosti i Gaza*, Vol. 4, May–June 1993, pp. 174–183.

[10] Azarova, O., Grudnitsky, V., and Kolesnichenko, Y., "Some Gas Dynamic Aspects of Flow Control by MW Energy Deposition," *Sixth Workshop on Magneto- Plasma-Aerodynamics for Aerospace Applications*, Inst. for High Temperatures, Moscow, 2005, pp. 152–163.

[11] Farzan, F., Knight, D., Azarova, O., and Kolesnichenko, Y., "Interaction of a Microwave Filament and Blunt Body in Supersonic Flow," AIAA, Paper No. 2008-1356, Jan. 2008.

[12] Khmara, D., Kolesnichenko, Y., and Knight, D., "A Kinetic Model of Microwave Energy Deposition in Air," *Fifth Workshop on Thermochemical Processes in Plasmadynamics*, edited by A. Kuranov, Lorentz Inst., St. Petersburg, Russia, June 2006, pp. 37–38.

[13] Raizer, Y. P., *Gas Discharge Physics*, 2nd ed., Springer–Verlag, New York, 1997.

[14] Khmara, D., Kolesnichenko, Y., and Knight, D., "Modeling of Microwave Filament Origination," AIAA Paper 2006-0794, Jan. 2006.

[15] Kolesnichenko, Y., Brovkin, V., Leonov, S., Krylov, A., Lashkov, V., Mashek, I., Gorynya, A., and Ryvkin, M., "Investigation of AD-Body Interaction with Microwave Discharge Region in Supersonic Flows," AIAA Paper 2001-0345, Jan. 2001.

[16] Molvik, G., and Merkle, C., "A Set of Strongly Coupled, Upwind Algorithms for Computing Flows in Chemical Nonequilibrium," AIAA Paper 89-0199, Jan. 1989.

[17] Zhong, X., "Additive Semi-Implicit Runge-Kutta Methods for Computing High-Speed Nonequilibrium Reactive Flows," *Journal of Computational Physics*, Vol. 128, No. 1, Oct. 1996, pp. 19–31. doi:10.1006/jcph.1996.0193

[18] Gropp, W., Lusk, E., Ashton, D., Balaji, P., Buntinas, D., Butler, R., Chan, A., Krishna, J., Mercier, G., Ross, R., Thakur, R., and Toonen, B., MPICH2 User's Guide, Ver. 1.0.5, Argonne National Lab., Argonne, IL, Dec. 2006.

[19] Georgievsky, P., and Levin, V., "Bow Shock Wave Structures Control by Pulse-Periodic Energy Input," AIAA Paper 2004-1019, Jan. 2004.

[20] Popov, N., "Investigation of the Mechanism for Fast Air Heating in Gas Discharges," *Proceedings of the Fourth Workshop on Magneto-Plasma Aerodynamics in Aerospace Applications*, edited by V. Bityurin, Joint Inst. of High Temperatures, Moscow, 2002, pp. 254–260.

[21] Slanger, T., and Black, G., "Electronic-to-vibrational Energy Transfer Efficiency in the $O(^1D) - N_2$ and $O(^1D) - CO$ Systems," *Journal of Chemical Physics*, Vol. 60, 1974, pp. 468–477. doi:10.1063/1.1681064

[22] Kella, D., Johnson, P., Pedersen, H., Vejby-Christensen, L., and Andersen, L., "Branching Ratios for Dissociative Recombination of $^{15}N^{14}N^+$," *Physical Review Letters*, Vol. 77, No. 12, Sept. 1996, pp. 2432–2435. doi:10.1103/PhysRevLett.77.2432

[23] Peterson, J., Le Padellec, A., Danared, H., Dunn, G., Larsson, M., Larson, A., Peverall, R., Strömholm, C., Rosén, S., Ugglas, M., and van der Zande, W., "Dissociative Recombination and Excitation of N_2^+: Cross Sections and Product Branching Ratios," *Journal of Chemical Physics*, Vol. 108, No. 5, 1998, pp. 1978–1988. doi:10.1063/1.475577

[24] van der Zande, W., Peverall, R., Rosén, S., Peterson, J., and Larsson, M., "Dissociatieve Recombinatie Van N_2^+ Bestudeerd in de Zware Ionen Opslag Ring CRYRING in Stockholm," *Van A tot Q*, Vol. 12, 1997–1998, pp. 73–80.

[25] Guberman, S., "$O(^1D)$ from the Dissociative Recombination of O_2^+," *American Physical Society AAPT Joint Meeting, APS Meeting Abstracts*, American Physical Society, College Park, MD, April 1997, p. D1556.

[26] Kolesnichenko, Y., Brovkin, V., Khmara, D., Lashkov, V., Mashek, I., and Ryvkin, M., "Fine Structure of Microwave Discharge: Evolution Scenario," AIAA Paper 2003-0362, Jan. 2003.

X. Zhong
Associate Editor